

Mathematical Modeling and Stability Analysis of Delay Differential Equations

Zaid Ahsan

A Thesis Submitted to
Indian Institute of Technology Hyderabad
In Partial Fulfillment of the Requirements for
The Degree of Master of Technology



भारतीय प्रौद्योगिकी संस्थान हैदराबाद
Indian Institute of Technology Hyderabad

Department of Mechanical and Aerospace Engineering

June 2015

Declaration

I declare that this written submission represents my ideas in my own words, and where ideas or words of others have been included, I have adequately cited and referenced the original sources. I also declare that I have adhered to all principles of academic honesty and integrity and have not misrepresented or fabricated or falsified any idea/data/fact/source in my submission. I understand that any violation of the above will be a cause for disciplinary action by the Institute and can also evoke penal action from the sources that have thus not been properly cited, or from whom proper permission has not been taken when needed.



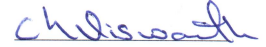
(Signature)

(Zaid Ahsan)

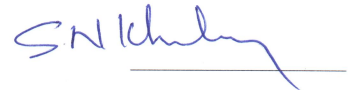
(Roll No. ME10B14M000006)

Approval Sheet

This Thesis entitled Mathematical Modeling and Stability Analysis of Delay Differential Equations by Zaid Ahsan is approved for the degree of Master of Technology from IIT Hyderabad



(Dr. Viswanath Chinthapenta) Examiner
Dept. of Mechanical and Aerospace Engineering, IITH



(Dr. Syed Nizamuddin Khaderi) Examiner
Dept. of Mechanical and Aerospace Engineering, IITH



(Dr. Chandrika Prakash Vyasarayani) Adviser
Dept. of Mechanical and Aerospace Engineering, IITH



(Dr. N. R. Aravind) Chairman
Dept. of Computer Science and Engineering, IITH

Acknowledgements

I would like to express my gratitude to all those who helped me to finish my thesis. First and foremost I would like to thank God, the almighty, for giving me strength and courage to do research.

I would like to thank my parents and siblings for their love, endless support and encouragement.

I express my sincere gratitude to my supervisor Dr. V. C. Prakash for his inspiration, valuable guidance, timely suggestions and constant encouragement during each and every phase of this work.

Finally, I would like to thank all my friends Anwar, Sumit, Amit, Rajesh, Sammed, Harilal and Ikhlaas for supporting me to finish my work.

Dedication

*This thesis is dedicated to my parents & siblings
for their love, endless support
and encouragement*

Abstract

Finite-dimensional approximations are developed for retarded delay differential equations (DDEs). The DDE system is equivalently posed as an initial–boundary value problem consisting of hyperbolic partial differential equations (PDEs). By exploiting the equivalence of partial derivatives in space and time, we develop a new PDE representation for the DDEs that is devoid of boundary conditions. The resulting boundary condition–free PDEs are discretized using the Galerkin method with Legendre polynomials as the basis functions, whereupon we obtain a system of ordinary differential equations (ODEs) that is a finite-dimensional approximation of the original DDE system. We present several numerical examples comparing the solution obtained using the approximate ODEs to the direct numerical simulation of the original nonlinear DDEs. Stability charts developed using our method are compared to existing results for linear DDEs. The presented results clearly demonstrate that the equivalent boundary condition–free PDE formulation accurately captures the dynamic behaviour of the original DDE system.

As a second work, we study the stability of human balance during stance using inverted single- and double-pendulum models, accounting for physiological reflex delays in the controller. The governing second-order neutral delay differential equation (NDDE) is transformed into an equivalent partial differential equation constrained by a boundary condition, then into a system of ordinary differential equations (ODEs) using the Galerkin method. The stability of the ODE system approximates that of the original NDDE system; convergence is achieved by increasing the number of terms used in the Galerkin approximation. We validate our formulation by deriving analytical expressions for the stability margins of the double-pendulum human stance model. Numerical examples demonstrate that proportional–derivative–acceleration feedback generally, but not always, results in larger stability margins than proportional–derivative feedback in the presence of reflex delays.

Contents

Declaration	ii
Approval Sheet	iii
Acknowledgements	iv
Abstract	vi
1 Introduction	1
1.1 Literature review	2
1.2 Thesis structure	3
2 Embedded boundary method for Retarded Delay Differential Equations	5
2.1 Mathematical modeling	5
2.2 Embedded boundary method	6
2.3 Tau method	8
2.4 Lagrange Multiplier method	9
2.5 Numerical Studies	10
2.5.1 Coupled First-order DDEs	10
2.5.2 Second-order DDE	10
2.5.3 Stability charts	12
2.6 Relationship between Embedded boundary and Lagrange multiplier	14
2.7 Application to control	15
3 Galerkin Methods for stability analysis with application to Bio-Mechanics	17
3.1 Mathematical Modeling	17
3.2 Results and Discussion	20
3.2.1 Single-pendulum human stance model	20
3.2.2 Double-pendulum human stance model	22
3.3 Limitations of the Analytical Approach	27
4 Conclusions	31
References	33

Chapter 1

Introduction

Mathematical models involving delay differential equations (DDEs) [1] are used to represent time-delay effects in a wide range of engineering systems. Examples include control systems [2], machine tool vibration [3, 4], fluid–structure interaction [5], and traffic flow modelling [6].

The infinite-dimensional nature of DDEs complicates their analysis. We can always pose a DDE as an equivalent hyperbolic partial differential equation (PDE) constrained by a nonlinear boundary condition [7–9]. The mathematical representation of the PDE system appears to be more complicated than that of the original DDE; however, several methods are available for converting the PDE into a system of simple ordinary differential equations (ODEs) [10]. We, thus, arrive at a finite-dimensional ODE approximation of the original DDE, and can then make use of existing algorithms for the integration and continuation of these ODEs [11, 12]. Therein lies the benefit of this approach: by converting DDEs into systems of ODEs, we can exploit all existing tools developed for ODE systems to analyze the original DDEs.

Galerkin methods [10] are considered to be the optimal choice for obtaining reduced-order models for PDEs; however, in the case of a DDE-equivalent PDE, one must also handle the nonlinear boundary condition. Once a PDE has been discretized, the boundary condition can be incorporated using a Lagrange multiplier [13] or by employing the tau method [7, 14, 15]. In this work, we propose a formulation in which the boundary condition is completely eliminated and embedded directly into the PDE. Consequently, no special treatment of the boundary condition is necessary when applying the Galerkin method.

As a second work, we study a problem of bio mechanics. Persons aged 60 and over represent the fastest-growing sector of the worldwide population—a great triumph of humanity, but also a great economic challenge. In persons aged 65 and over, falling is the leading cause of both fatal and nonfatal injury [16], with approximately 28–36% of persons in this cohort falling each year [17]. In 2000, falls among the elderly in the United States accounted for over \$19 billion in direct medical costs [18]; this economic burden is expected to increase in the future. A deeper understanding of human balance will contribute to improving the quality and longevity of life for the elderly, while reducing healthcare costs for hospitalization and rehabilitation resulting from falls.

In this work, we model the human as a double inverted pendulum in the sagittal plane, with controllers at both the ankle and hip. Due to the reflex delay and acceleration feedback in the model, the governing dynamic equation is a neutral delay differential equation (NDDE)—that is,

the equation takes the form of a DDE with a delayed argument in the highest-order derivative. Thus, the stability of human balance during stance must be determined by analyzing the stability region of an NDDE [19]. Unfortunately, NDDEs are infinite-dimensional systems and, as such, their characteristic equations are quasi-polynomials with an infinite number of roots—all of which must lie in the left half-plane if the NDDE is to be stable. Insperger et al. obtained analytical results by inspecting the characteristic equation of the single-pendulum NDDE directly. Here, we extend their strategy to the analysis of a double inverted pendulum, and use symbolic computational techniques to obtain analytical expressions for the stability margins of this more complex model. We also apply an approximate method [20] to analyze the stability of second-order NDDEs by first transforming the NDDE into an equivalent partial differential equation (PDE) constrained by a boundary condition, then converting the PDE into a system of ordinary differential equations (ODEs) using the Galerkin method. Comparison between the analytical and numerical results demonstrates that the stability of the ODE system approximates that of the original NDDE system, and convergence is achieved by increasing the number of terms used in the Galerkin approximation.

We first apply our numerical Galerkin approach to obtain the stability diagrams for a single-pendulum human model with reflex delay, controlled using both PD and PDA feedback control strategies [21]. We compare our results with those obtained by Insperger et al. [21] to validate the developed method. We then use the same strategy as Insperger et al. to derive analytical expressions for the stability margins of the double inverted pendulum model. Next, we apply our numerical technique to a double-pendulum model with reflex delay, and perform numerical experiments to compare the Galerkin and analytical methods. We also seek to determine whether a PDA controller provides a larger stability region than a PD controller for this more complex model. Our results indicate that the stability margins obtained with the Galerkin and analytical approaches are in excellent agreement, and that PDA feedback generally remains superior to PD feedback when motion at the hip is considered.

In the next section, we discuss the literature review for obtaining an approximate solution to constant coefficient DDEs and the stability of human model during stance (sagittal plane).

1.1 Literature review

Many methods have been proposed in literature to obtain an approximate solution to constant coefficient DDEs and to analyze their stability. In this section, however we only review papers that have been most relevant to our work. Kalmár-Nagy [22] used the method of steps and inverse Laplace transform to determine the stability regions for higher order constant coefficient DDEs. Ulsoy et al developed the Lambert W function method to obtain analytical solutions for scalar first order DDE, which was later extended to matrix Lambert W function to solve system of linear DDEs [23].

It is very well known that the infinite dimensional nature of the DDEs complicates their analysis. Maset [9] obtained a finite dimensional ODE approximation of constant coefficient linear DDEs by posing them as abstract Cauchy problem. The transformation proposed by Maset converts the original DDE into an equivalent hyperbolic PDE constrained by a boundary condition, which is then discretized into a system of ODEs using the method of lines. Koto [8] also used the same Cauchy transformation to numerically solve initial value problem DDEs by posing them as initial boundary value problem.

The application of Galerkin methods to project a DDE into an approximated system of finite dimensional ODEs was discussed very first in detail by Wahi et al [7]. They first transform the DDEs into an equivalent PDE system constrained by a boundary condition, which may be nonlinear. The resulting PDE system is then finally truncated into a finite dimensional system of ODEs using Galerkin projections. To incorporate the ODE corresponding to the boundary condition, they use the tau method in which the last row of the system ODEs is replaced by the boundary condition. A notable point of this method is that it can be used for both linear as well as nonlinear DDEs. An interested reader is referred to their paper to get a detailed understanding of the technique. Vyasarayani [13] also developed a method based on Galerkin projections to obtain ODE approximations for higher order DDEs and proposed the use of Langrange multipliers to enforce the nonlinear boundary constraints.

Thus, we see that in obtaining finite dimensional ODE approximation of DDEs, the boundary condition must be handled explicitly. They are incorporated into the system ODEs either using Tau or the Langrange multiplier technique. However, we observed that using the equivalence of partial derivatives at the boundary, we can directly incorporate the PDE corresponding to the boundary condition into the system PDE, and obtain boundary free ODE approximations to the DDE.

As a second work, we focus on the stability of human balance during quiet standing, which is often studied using a single inverted pendulum [24]. An inverted pendulum is inherently unstable, and can remain upright only when assisted by a controller [25]. Similarly, humans use their muscles to apply control torques about the ankle, again to stabilize an otherwise unstable system. Note, however, that the control torques applied by humans are intermittent: there is substantial reflex delay between detecting a loss of balance and generating muscle forces [26, 27] due to delays in the human sensing, processing, and actuation systems [28, 29]. It has recently been shown that the strategy used by humans to maintain stability cannot be proportional-derivative (PD) control, relying on proprioceptive [30] and visual sensors alone, since the required control gains correspond to forces that exceed the capabilities of human muscles [31]. A recent study by Insperger et al. [21] suggests that humans instead use a proportional-derivative-acceleration (PDA) control strategy, aided by the acceleration feedback signal generated within the vestibular system [32]. Insperger et al. established that PDA control provides a larger stability margin than PD control when applied to a single-pendulum model. There is some debate as to whether a single inverted pendulum is an adequate representation of a human when standing, since there is also considerable angular motion at the hip during postural sway [31]. In this work, we model the human as a double inverted pendulum in the sagittal plane, with controllers at both the ankle and hip and compare the PD and PDA stability margins.

1.2 Thesis structure

The entire thesis has been divided in four chapters. The first chapter is the introduction, wherein we discuss the application of delay differential equations, the different types of DDEs such as constant coefficient or time periodic DDEs, and a brief overview of the method proposed in the thesis to model them. We then discuss the different methods proposed in literature to obtain an approximate solution to the system of DDEs. Finally, we define the problem that we are going to focus on. In the second

chapter, we first discuss the mathematical modeling of DDEs and propose our embedded boundary method for retarded DDEs. Next we discuss the tau and lagrange multiplier techniques, the two popular methods to model DDEs. Finally, we present several numerical examples to demonstrate the efficacy of the proposed method. In the third chapter, we present the application of Galerkin methods to a problem of bio-mechanics. First we model the governing equation of the single-pendulum human stance model during stance using the Galerkin method and compare the obtained stability margins with the analytical results. Then we extend this strategy and derive analytical stability margins for the double- pendulum model and compare them with the Galerkin results. Finally conclusions are provided in chapter 4.

Chapter 2

Embedded boundary method for Retarded Delay Differential Equations

In this chapter, we propose the embedded boundary method for obtaining approximate solutions to DDEs. In the first section, we discuss the mathematical modeling of the DDEs. First we present the class of DDEs in which we are interested in, and the equivalent PDE representation of the DDE. We then propose our embedded boundary method to obtain boundary free ODE approximations of the DDE. Next for the sake of comparison, we discuss the tau and Lagrange multiplier methods, the already existing techniques to obtain approximate solutions to DDEs. In the next section, we present the approximate solution and stability charts using the proposed embedded boundary method for first and second order DDEs. We also discuss an interesting relationship between the embedded boundary and the Lagrange multiplier method. Finally, we present the application of our proposed method on a control problem.

2.1 Mathematical modeling

Consider the following system of n first-order DDEs:

$$\dot{z}_i = f_i(\mathbf{p}, \mathbf{q}_i, t), \quad i = 1, 2, \dots, n, \quad (2.1)$$

where $\mathbf{p} = [z_1, z_2, \dots, z_n]$ and $\mathbf{q}_i = [z_1(t - \alpha_{i1}), z_2(t - \alpha_{i2}), \dots, z_n(t - \alpha_{in})]$. The delays are $\alpha_i = [\alpha_{i1} > 0, \alpha_{i2} > 0, \dots, \alpha_{in} > 0]$, $i = 1, 2, \dots, n$ and the initial functions are $z_i(t) = \psi_i(t)$, $-\alpha_{im} \leq t \leq 0$, $i = 1, 2, \dots, n$; α_{im} is the maximum delay appearing in $z_i(t)$. Since the delay argument does not appear in the highest-derivative term, (2.1) is referred to as a retarded DDE. We introduce the following standard transformation [8, 9]:

$$y_i(s, t) \triangleq z_i(t + s), \quad (2.2)$$

and convert the DDE system (2.1) and its history functions into the following equivalent initial-boundary value problem:

$$\frac{\partial y_i}{\partial t} = \frac{\partial y_i}{\partial s}, \quad t \geq 0, \quad -\alpha_{im} \leq s \leq 0 \quad (2.3a)$$

$$\left. \frac{\partial y_i(s, t)}{\partial t} \right|_{s=0} = f_i(\mathbf{u}, \mathbf{v}_i, t) \quad (2.3b)$$

$$y_i(s, 0) = \psi_i(s), \quad (2.3c)$$

where

$$\mathbf{u} = [y_1(0, t), y_2(0, t), \dots, y_n(0, t)] \quad (2.4a)$$

$$\mathbf{v}_i = [y_1(-\alpha_{i1}, t), y_2(-\alpha_{i2}, t), \dots, y_n(-\alpha_{in}, t)]. \quad (2.4b)$$

Here, $y_i(0, t)$ represents the solution to the DDE (2.1) when $s = 0$. Several methods have been proposed in the literature to incorporate the boundary condition (2.3b) when discretizing the PDE (2.3a), such as the Lagrange multiplier and tau methods.

2.2 Embedded boundary method

We now present our procedure for embedding the boundary condition into the PDE, thereby eliminating the boundary condition from the formulation. We first rewrite (2.3b) exploiting the equivalence of partial derivatives in space and time (2.3a):

$$\frac{\partial y_i(0, t)}{\partial s} - f_i(\mathbf{u}, \mathbf{v}_i, t) = 0. \quad (2.5)$$

Next, we combine the PDE (2.3a) and the modified boundary condition (2.5):

$$\frac{\partial y_i}{\partial t} = \frac{\partial y_i}{\partial s} + \left(\frac{\partial y_i(0, t)}{\partial t} - f_i(\mathbf{u}, \mathbf{v}_i, t) \right) c\delta(s), \quad (2.6)$$

where $\delta(s)$ is the Dirac delta function and c is the boundary contribution parameter, which is assumed to be 1. We can see that collocating the PDE at any point on the domain $-\alpha_{im} \leq s < 0$ satisfies (2.3a), and by collocating at the boundary $s = 0$, we recover the boundary condition (2.5). We now assume an N -term series solution $y_i(s, t)$ for the PDE:

$$y_i(s, t) = \phi_i(s)^\top \eta_i(t), \quad (2.7)$$

where $\phi_i(s) = [\phi_1(s), \phi_2(s), \dots, \phi_N(s)]^\top$ are the global shape functions and $\eta_i(t) = [\eta_{i1}(t), \eta_{i2}(t), \dots, \eta_{iN}(t)]^\top$ are the independent coordinates. Shifted Legendre polynomials are used as global shape functions:

$$\phi_1(s) = 1 \quad (2.8a)$$

$$\phi_2(s) = 1 + \frac{2s}{\tau} \quad (2.8b)$$

$$\phi_i(s) = \frac{(2i-3)\phi_2(s)\phi_{i-1}(s) - (i-2)\phi_{i-2}(s)}{i-1}, \quad i = 3, 4, \dots, N. \quad (2.8c)$$

In retarded DDEs, where the order of the delayed arguments is less than that of the highest-order derivative, the solution will become smoother with every knot. If the solution is C^0 -continuous at time $t=0$, for example, the solution will be C^1 -continuous after time $t = \tau$ (the first knot) and C^n -continuous after n knots [33]. Retarded DDEs always eventually become smooth, which is the reason this approximation is effective.

Upon substituting the series solution (2.7) into (2.6), we obtain the following:

$$\boldsymbol{\phi}_i(s)^\top \dot{\boldsymbol{\eta}}_i(t) = \boldsymbol{\phi}'_i(s)^\top \boldsymbol{\eta}_i(t) + \left(\boldsymbol{\phi}_i(0)^\top \dot{\boldsymbol{\eta}}_i(t) - f_i(\mathbf{u}, \mathbf{v}_i, t) \right) \delta(s), \quad i = 1, 2, \dots, n, \quad (2.9)$$

where $\boldsymbol{\phi}'_i(s) \equiv \partial \boldsymbol{\phi}_i(s) / \partial s$. Finally, we pre-multiply both sides of (2.9) by $\boldsymbol{\phi}_i(s)$, integrate over the domain $s \in [-\alpha_{im}, 0]$, and collect the terms involving $\dot{\boldsymbol{\eta}}_i(t)$ to obtain a system of ODEs:

$$\mathbf{M}_i \dot{\boldsymbol{\eta}}_i(t) = \mathbf{K}_i \boldsymbol{\eta}_i(t) - \boldsymbol{\phi}_i(0) f_i(\mathbf{u}, \mathbf{v}_i, t), \quad i = 1, 2, \dots, n, \quad (2.10)$$

where

$$\mathbf{M}_i = \int_{-\alpha_{im}}^0 \boldsymbol{\phi}_i(s) \boldsymbol{\phi}_i(s)^\top \mathrm{d}s - \boldsymbol{\phi}_i(0) \boldsymbol{\phi}_i(0)^\top \triangleq \mathbf{A}_i - \boldsymbol{\phi}_i(0) \boldsymbol{\phi}_i(0)^\top \quad (2.11a)$$

$$\mathbf{K}_i = \int_{-\alpha_{im}}^0 \boldsymbol{\phi}_i(s) \boldsymbol{\phi}'_i(s)^\top \mathrm{d}s. \quad (2.11b)$$

The use of shifted Legendre polynomials as global shape functions allows us to write the entries of matrices \mathbf{A}_i and \mathbf{K}_i in closed form as follows:

$$\mathbf{A}_{cd} = \frac{\alpha_{im}}{2c-1} \delta_{cd} \quad c = 1, 2, \dots, N; d = 1, 2, \dots, N \quad (2.12a)$$

$$\mathbf{K}_{cd} = \begin{cases} 2, & \text{if } c < d \text{ and } c + d \text{ is odd} \\ 0, & \text{otherwise} \end{cases} \quad c = 1, 2, \dots, N; d = 1, 2, \dots, N. \quad (2.12b)$$

In (2.10), the term $f_i(\mathbf{u}, \mathbf{v}_i, t)$ can be obtained by substituting the series solution (2.7) into the expressions for \mathbf{u} and \mathbf{v}_i (2.4): We now determine the initial conditions for the ODE system.

$$\mathbf{u} = \left[\boldsymbol{\phi}_1(0)^\top \boldsymbol{\eta}_1(t), \boldsymbol{\phi}_2(0)^\top \boldsymbol{\eta}_2(t), \dots, \boldsymbol{\phi}_n(0)^\top \boldsymbol{\eta}_n(t) \right] \quad (2.13a)$$

$$\mathbf{v}_i = \left[\boldsymbol{\phi}_1(-\alpha_{i1})^\top \boldsymbol{\eta}_1(t), \boldsymbol{\phi}_2(-\alpha_{i2})^\top \boldsymbol{\eta}_2(t), \dots, \boldsymbol{\phi}_n(-\alpha_{in})^\top \boldsymbol{\eta}_n(t) \right]. \quad (2.13b)$$

We now substitute the series solution (2.7) into the initial conditions (2.3c):

$$\psi_i(s) = \boldsymbol{\phi}_i^\top(s) \boldsymbol{\eta}_i(0), \quad i = 1, 2, \dots, n. \quad (2.14)$$

Finally, we pre-multiply both sides of (2.14) by $\boldsymbol{\phi}_i(s)$ and integrate over the domain $s \in [-\alpha_{im}, 0]$ to obtain the following initial conditions for the ODE system:

$$\boldsymbol{\eta}_i(0) = \mathbf{A}_i^{-1} \int_{-\alpha_{im}}^0 \boldsymbol{\phi}_i(s) \psi_i(s) \mathrm{d}s, \quad i = 1, 2, \dots, n, \quad (2.15)$$

where \mathbf{A}_i is defined in (2.11a). Thus, we have converted the original DDE (2.1) into a system of ODEs (2.10) with initial conditions given by (2.15). The ODEs can be solved numerically to obtain

$\boldsymbol{\eta}_i(t)$, whereupon an approximate solution for the DDE (2.1) can be obtained as follows:

$$y_i(0, t) = \eta_{i0}(t) = \boldsymbol{\phi}_i(0)^\top \boldsymbol{\eta}_i(t). \quad (2.16)$$

We define the following error metric to quantify how well the solutions of (2.6) satisfy the original boundary conditions (2.3b):

$$e_i(t) = \left. \frac{\partial y_i}{\partial t} \right|_{0,t} - f_i = \boldsymbol{\phi}_i(0)^\top \dot{\boldsymbol{\eta}}_i(t) - f_i, \quad i = 1, 2, \dots, n. \quad (2.17)$$

In the sequel, we use a 2-norm to establish the error associated with all boundary conditions:

$$e(t) = \sqrt{e_1(t)^2 + e_2(t)^2 + \dots + e_n(t)^2}. \quad (2.18)$$

We now compare the proposed formulation to the tau and Lagrange multiplier techniques, the two most common strategies for obtaining approximate solutions to DDEs.

2.3 Tau method

In this method, the series solution (2.7) is first substituted into the equivalent system of PDEs (2.3a),

$$\boldsymbol{\phi}_i(s)^\top \dot{\boldsymbol{\eta}}_i(t) = \boldsymbol{\phi}'_i(s)^\top \boldsymbol{\eta}_i(t) \quad i = 1, 2, \dots, n, \quad (2.19)$$

Pre-multiplying both sides with $\boldsymbol{\phi}_i(s)$ and integrating over the domain $s \in [-\alpha_{im}, 0]$, we obtain the following ODEs:

$$\mathbf{A}_i \dot{\boldsymbol{\eta}}_i(t) = \mathbf{K}_i \boldsymbol{\eta}_i(t) \quad i = 1, 2, \dots, n, \quad (2.20)$$

where \mathbf{A}_i and \mathbf{K}_i are the same as defined in (2.12a) and (2.12b) respectively. Next we substitute the series solution (2.7) into the boundary condition (2.3b) to obtain,

$$\boldsymbol{\phi}_i(s)^\top \dot{\boldsymbol{\eta}}_i(t) = f_i(\mathbf{u}, \mathbf{v}_i, t) \quad i = 1, 2, \dots, n, \quad (2.21)$$

and the expressions of \mathbf{u}, \mathbf{v}_i are obtained as:

$$\mathbf{u} = \left[\boldsymbol{\phi}_1(0)^\top \boldsymbol{\eta}_1(t), \boldsymbol{\phi}_2(0)^\top \boldsymbol{\eta}_2(t), \dots, \boldsymbol{\phi}_n(0)^\top \boldsymbol{\eta}_n(t) \right] \quad (2.22a)$$

$$\mathbf{v}_i = \left[\boldsymbol{\phi}_1(-\alpha_{i1})^\top \boldsymbol{\eta}_1(t), \boldsymbol{\phi}_2(-\alpha_{i2})^\top \boldsymbol{\eta}_2(t), \dots, \boldsymbol{\phi}_n(-\alpha_{in})^\top \boldsymbol{\eta}_n(t) \right]. \quad (2.22b)$$

The boundary condition (2.21) is then incorporated to the ODEs (2.20) by replacing the last row of \mathbf{A}_i and \mathbf{K}_i in (2.20) with the boundary condition. Thus, finally we arrive at the following system of ODEs:

$$\mathbf{A}_{iTau} \dot{\boldsymbol{\eta}}_i(t) = \mathbf{K}_{iTau} \boldsymbol{\eta}_i(t) + \mathbf{F}_i \quad i = 1, 2, \dots, n, \quad (2.23)$$

where $\mathbf{A}_{iTau} = \begin{bmatrix} \bar{\mathbf{A}}_i \\ \boldsymbol{\phi}(0)^\top \end{bmatrix}$, $\mathbf{K}_{iTau} = \begin{bmatrix} \bar{\mathbf{K}}_i \\ 0 \end{bmatrix}$ and $\mathbf{F}_i = \begin{bmatrix} \vdots \\ f_i(\mathbf{u}, \mathbf{v}_i, t) \end{bmatrix}$.

Here $\bar{\mathbf{A}}_i$ and $\bar{\mathbf{K}}_i$ are obtained by deleting the last row of \mathbf{A}_i and \mathbf{K}_i , and \mathbf{F}_i is a column vector

whose all entries are zero except the last one. The initial condition for Eq. (2.23) is given by

$$\boldsymbol{\eta}_i(0) = \mathbf{A}_i^{-1} \int_{-\alpha_{im}}^0 \boldsymbol{\phi}_i(s) \psi_i(s) \, ds, \quad i = 1, 2, \dots, n, \quad (2.24)$$

Finally the system of ODEs (2.23) is then integrated forward in time to obtain an approximate solution to the DDEs (2.1). The approximate solution is obtained as:

$$y_i(0, t) = \eta_{i0}(t) = \boldsymbol{\phi}_i(0)^T \boldsymbol{\eta}_i(t). \quad (2.25)$$

2.4 Lagrange Multiplier method

Another widely used method to obtain an approximate solution to the DDEs is the Lagrange multiplier method. In this method, the boundary constraint (2.3b) is enforced using Lagrange multipliers. Firstly, the PDE (2.3a) is written as:

$$\frac{\partial y_i}{\partial t} = \frac{\partial y_i}{\partial s} + \delta(s) \gamma_i(t), \quad i = 1, 2, \dots, n \quad (2.26)$$

Here $\gamma_i(t)$ denotes the lagrange multiplier, which is time dependent. On substituting the series solution (2.7) in (2.26), we obtain

$$\boldsymbol{\phi}_i(s)^T \dot{\boldsymbol{\eta}}_i(t) = \boldsymbol{\phi}_i'(s)^T \boldsymbol{\eta}_i(t) + \delta(s) \gamma_i(t), \quad i = 1, 2, \dots, n \quad (2.27)$$

Pre-multiplying both sides of (2.27) with $\boldsymbol{\phi}_i(s)$ and integrating over the domain $(-\alpha_{im} \leq s \leq 0)$ yields

$$\mathbf{A}_i \dot{\boldsymbol{\eta}}_i(t) = \mathbf{K}_i \boldsymbol{\eta}_i(t) + \boldsymbol{\phi}_i(0) \gamma_i(t), \quad i = 1, 2, \dots, n \quad (2.28)$$

where \mathbf{A}_i and \mathbf{K}_i are the same as defined in (2.12a) and (2.12b) respectively. Now substituting the series solution (2.7) into the boundary condition (2.3b) results in,

$$\boldsymbol{\phi}_i(0)^T \dot{\boldsymbol{\eta}}_i(t) = f_i(\mathbf{u}, \mathbf{v}_i, t), \quad i = 1, 2, \dots, n \quad (2.29)$$

where \mathbf{u} and \mathbf{v}_i are the same as obtained in (2.4a) and (2.4b) respectively. We now use (2.28) and (2.29) to obtain the following expression for the lagrange multiplier($\gamma_i(t)$):

$$\gamma_i(t) = \frac{f_i(\mathbf{u}, \mathbf{v}_i, t)}{\boldsymbol{\phi}_i(0)^T [\mathbf{A}_i^{-1} \boldsymbol{\phi}_i(0)]} - \frac{\boldsymbol{\phi}_i(0)^T [\mathbf{A}_i^{-1} \mathbf{K}_i \boldsymbol{\eta}_i(t)]}{\boldsymbol{\phi}_i(0)^T [\mathbf{A}_i^{-1} \boldsymbol{\phi}_i(0)]}, \quad i = 1, 2, \dots, n \quad (2.30)$$

On substituting back the expression of ($\gamma_i(t)$) in (2.28) and using the initial condition $\boldsymbol{\eta}_i(0) = \mathbf{A}_i^{-1} \int_{-\alpha_{im}}^0 \boldsymbol{\phi}_i(s) \psi_i(s) \, ds$, we integrate the ODEs forward in time to get $\boldsymbol{\eta}_i(t)$. The approximation solution is then obtained as:

$$y_i(0, t) = \eta_{i0}(t) = \boldsymbol{\phi}_i(0)^T \boldsymbol{\eta}_i(t). \quad (2.31)$$

In summary, we have developed a method to convert a system of DDEs into a system of PDEs without any boundary conditions. The PDEs are discretized using the Galerkin method and converted into a system of ODEs, which can then be solved numerically. As will be demonstrated in Section 2.5, our approach satisfies the original boundary conditions with only small amounts of er-

ror, and produces results that compare favourably with those obtained using the tau and Lagrange multiplier methods.

2.5 Numerical Studies

In this section, we present four test cases to investigate the accuracy of the approximation method we propose. The developed theory is applied to systems of first- and second-order DDEs. The numerical results for the proposed method are obtained using the `ode15s` solver in Matlab, and are compared to those obtained by integrating the DDEs directly using the `dde23` [34] solver. Relative and absolute integration tolerances of 10^{-8} are used throughout.

2.5.1 Coupled First-order DDEs

Consider the following system of retarded DDEs:

$$\dot{z}_1(t) + b_1 z_1(t) + b_2 z_2(t) + b_3 z_1(t - \alpha_{11}) + b_4 z_2(t - \alpha_{12})^3 = 0 \quad (2.32a)$$

$$\dot{z}_2(t) + b_5 z_1(t) + b_6 z_2(t) + b_7 z_1(t - \alpha_{21}) + b_8 z_2(t - \alpha_{22})^3 = F \sin(\omega t). \quad (2.32b)$$

This is a nonlinear system of coupled DDEs containing delays in both z_1 and z_2 . The initial history functions are assumed to be the following:

$$z_1(t) = 0, \quad -\max(\alpha_{11}, \alpha_{21}) \leq t \leq 0 \quad (2.33a)$$

$$z_2(t) = 0, \quad -\max(\alpha_{12}, \alpha_{22}) \leq t \leq 0. \quad (2.33b)$$

In Figure 2.1, we compare the displacements $y_1(0, t)$ and $y_2(0, t)$ obtained using the Galerkin method to those obtained using the `dde23` solver in Matlab; the parameters are provided in the figure caption. Clearly, the results obtained using the Galerkin method match the direct numerical integration of (2.32). In Figure 2, we plot the least-square errors for $y_1(0, t)$ and $y_2(0, t)$ as functions of the number of terms used in the series approximation (2.7):

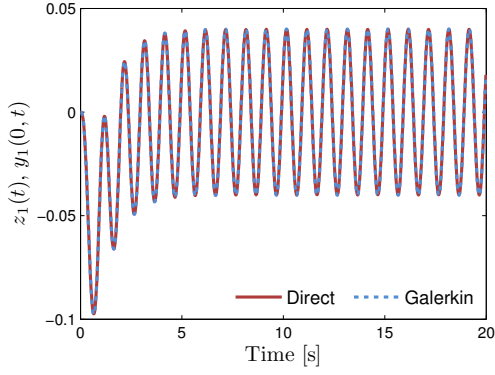
$$E_{LS} = \sum_{k=1}^{10000} (z(t_k) - y_1(0, t_k))^2. \quad (2.34)$$

The simulation was performed for $t \in [0, 100]$, which was divided into 10,000 equidistant points to compute the error (2.34). As shown in Figure 2.2, $N = 7$ terms are sufficient to achieve an error of 0.01. Also note that the error associated with all the methods decreases as N increases, indicating convergence.

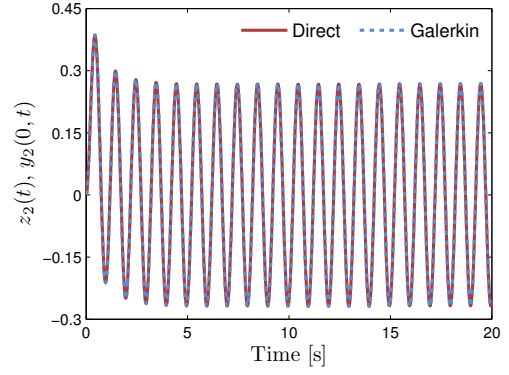
2.5.2 Second-order DDE

To test the developed formulation for higher-order DDEs, we now consider the following second-order nonlinear DDE:

$$\ddot{z}(t) + b_1 \dot{z}(t) + b_2 z(t) + b_3 z(t - \alpha)^3 + b_4 \dot{z}(t - \beta) = F \sin(\omega t), \quad (2.35)$$

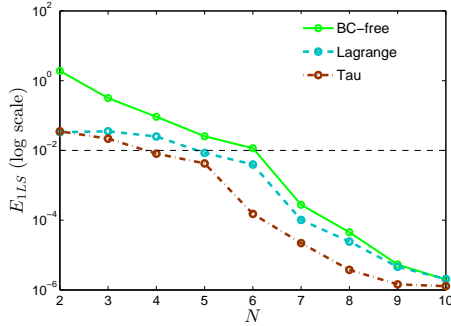


(a) $z_1(t)$ and $y_1(0, t)$.

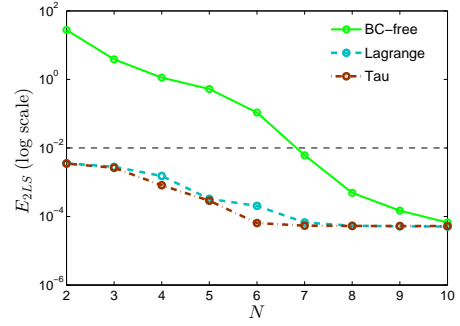


(b) $z_2(t)$ and $y_2(0, t)$.

Figure 2.1: Comparison of direct numerical solution $z_i(t)$ and solution obtained using the Galerkin method $y_i(0, t)$ for (2.32). The parameters are $b_1 = b_6 = 2$, $b_2 = b_4 = \alpha_4 = 1$, $b_3 = b_7 = b_8 = \alpha_1 = 0.1$, $b_5 = 0.75$, $\alpha_2 = 0.3$, $\alpha_3 = 0.5$, $F = 1.8$, $\omega = 2\pi$, and $N = 7$.



(a) $E_1 = \max(|z_1(t) - y_1(0, t)|)$.



(b) $E_2 = \max(|z_2(t) - y_2(0, t)|)$.

Figure 2.2: Maximum absolute error between direct numerical solution $z_i(t)$ and solution obtained using the Galerkin method $y_i(0, t)$ for (2.32) as frequency ω varies. Parameters are given in the caption for Figure 2.1.

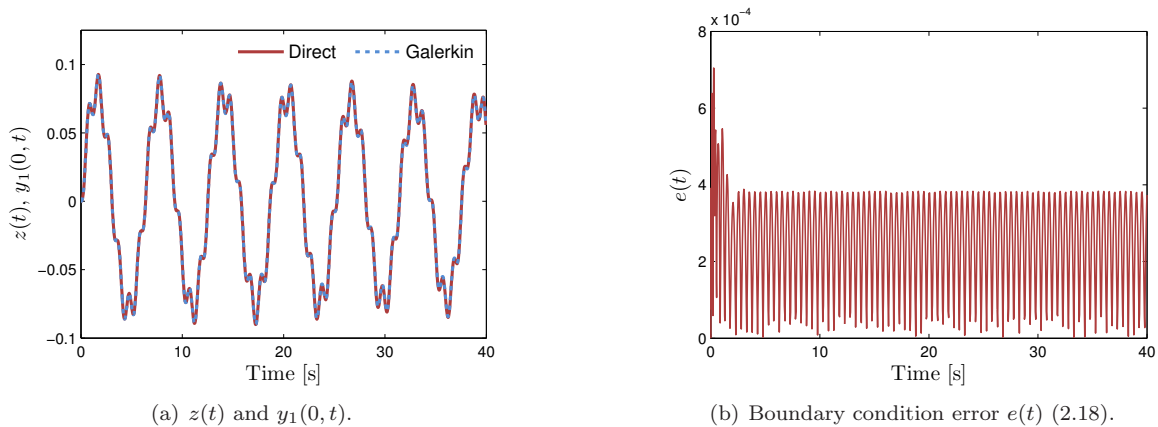


Figure 2.3: Comparison of direct numerical solution $z(t)$ and solution obtained using the Galerkin method $y_1(0,t)$ for (2.35). The parameters are $b_1 = 0.01$, $b_2 = b_3 = \alpha = 1$, $b_4 = 0$, $\beta = F = 0.5$, $\omega = 2\pi$, and $N = 7$.

which contains delays in both $z(t)$ and $\dot{z}(t)$. The initial history functions are assumed to be $z(t) = \dot{z}(t) = 0$, $-1 \leq t \leq 0$. In Figures 2.3, 2.4, and 2.5, we compare the displacement $y_1(0,t)$ obtained using the Galerkin method to that obtained using the `dde23` solver in Matlab using three sets of parameters (provided in the figure captions). In all three cases, the results obtained using the Galerkin method are in good agreement with the direct numerical integration of (2.35). In Figure 2.3(b), we show that the error associated with satisfying the boundary conditions is less than 8×10^{-4} using the first set of parameters; the absolute error is also low, as shown in Figure 2.4(b) for the second parameter set. In Figure 2.5(b), we plot the least-square error as a function of the number of terms N used in the series approximation (2.7):

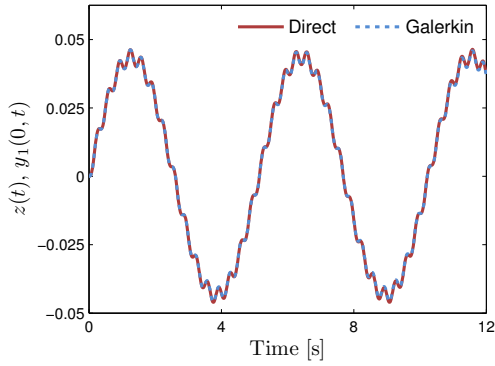
The simulation was performed for $t \in [0, 100]$, which was divided into 10,000 equidistant points to compute the error (2.34). As shown in Figure 2.5(b), convergence is achieved at $N = 11$, and the least-square error remains below 6×10^{-4} even when only 5 terms are retained in the series solution.

2.5.3 Stability charts

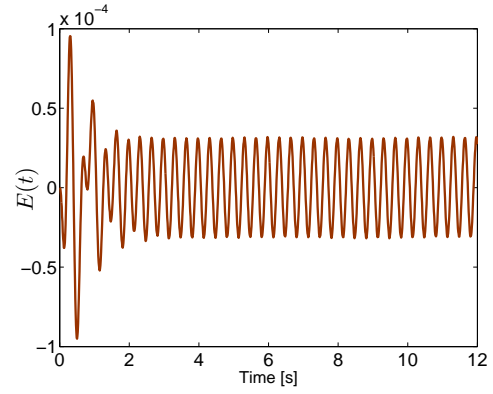
For linear DDEs, (2.10) takes the following form:

$$\dot{\boldsymbol{\eta}} = \mathbf{C}\boldsymbol{\eta}, \quad (2.36)$$

where $\boldsymbol{\eta} = [\boldsymbol{\eta}_1(t), \boldsymbol{\eta}_2(t), \dots, \boldsymbol{\eta}_n(t)]^\top$. The stability of linear DDEs can be analyzed by evaluating the stability of the ODEs obtained from the Galerkin approximation (2.36). The characteristic equation for a DDE is a quasi-polynomial with an infinite number of roots; to ascertain stability, we must determine whether all the roots have negative real parts. The roots of the characteristic equation can be found using a nonlinear solver; however, providing the solver with good initial guesses is a nontrivial task. In contrast, the Galerkin approximation of a linear DDE results in a system of ODEs of the form shown in (2.36), and we can directly evaluate the eigenvalues of these ODEs to establish system stability. In fact, the eigenvalues of (2.36) approximate the characteristic roots [35] of the original DDEs, and the approximation becomes increasingly accurate as the number of terms

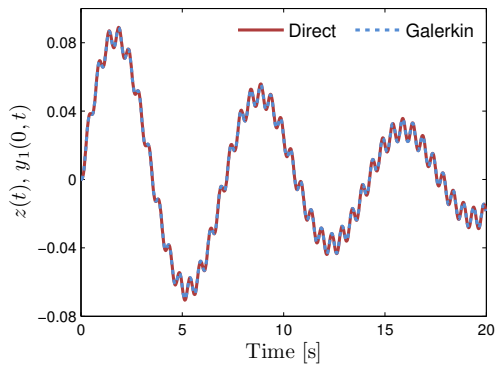


(a) $z(t)$ and $y_1(0, t)$.

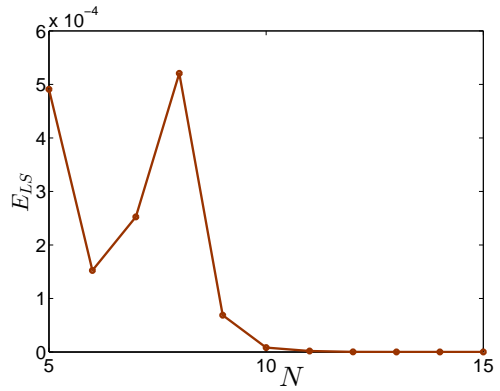


(b) Error $E(t) = z(t) - y_1(0, t)$.

Figure 2.4: Comparison of direct numerical solution $z(t)$ and solution obtained using the Galerkin method $y_1(0, t)$ for (2.35). The parameters are $b_1 = b_4 = 0$, $b_2 = 1.5$, $b_3 = 0.1$, $\alpha = F = 1$, $\beta = 0.5$, $\omega = 6\pi$, and $N = 7$.

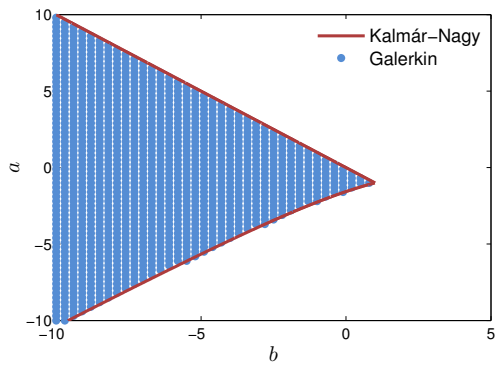


(a) $z(t)$ and $y_1(0, t)$ with $N = 7$.

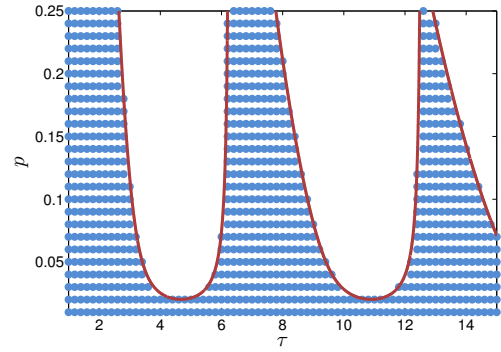


(b) Least-square error E_{LS} (2.34).

Figure 2.5: Comparison of direct numerical solution $z(t)$ and solution obtained using the Galerkin method $y_1(0, t)$ for (2.35) when the velocity delay term is nonzero. The parameters are $b_1 = 0.05$, $b_2 = 0.75$, $b_3 = \alpha = F = 1$, $b_4 = 0.1$, $\beta = 0.5$, and $\omega = 4\pi$.



(a) First-order system (2.37) with $\tau = 1$ and $N = 5$.



(b) Second-order system (2.38) with $\zeta = 0.01$ and $N = 25$.

Figure 2.6: Stability regions obtained analytically (red lines) and using the Galerkin method (blue dots) for first- and second-order systems.

in the series solution is increased. The system is stable if all eigenvalues of (2.36) have negative real parts.

Consider the following equation:

$$\dot{x}(t) = bx(t) + ax(t - \tau). \quad (2.37)$$

The stability of (2.37) changes as we vary parameters a and b . Figure 2.6(a) shows the stability diagram for (2.37) with $\tau = 1$. The region within the red lines is the stable region, as reported previously [22]; the blue dots indicate the same stable region, determined using the Galerkin method with $N = 5$. We have also studied the stability of a second-order system that arises in the study of machine tool vibration [36]:

$$\ddot{x}(t) + 2\zeta\dot{x}(t) + (1 + p)x(t) - px(t - \tau) = 0. \quad (2.38)$$

Figure 2.6(b) shows the stability diagram for (2.38) with $\zeta = 0.01$ as p and τ vary. The red lines indicate the stable region determined analytically [36]. Once again, the blue dots indicate that the same stable region is obtained using the Galerkin method.

2.6 Relationship between Embedded boundary and Lagrange multiplier

We now recall the proposed embedded boundary formulation(2.6):

$$\frac{\partial y}{\partial t} = \frac{\partial y}{\partial s} + \left(\frac{\partial y(0, t)}{\partial t} - f \right) c\delta(s)$$

We observed that for large values of the parameter c , the method approximates the Lagrange multiplier technique (2.4). To illustrate this point further, we plot the error between the numerical and the approximated solution for (2.5.2) using both the embedded boundary and the Lagrange

multiplier method. In Figure 2.7(a), we observe that with $c = 1$ the error using both the methods is very less, but Lagrange multiplier technique performs better than the embedded boundary method. However, in Figure 2.7(b) with $c = 1000$, we see that the error using the embedded boundary method exactly matches with that of Lagrange multipliers. Thus we can conclude that the embedded boundary method approximates the Lagrange multiplier technique for obtaining approximate solution of DDEs.

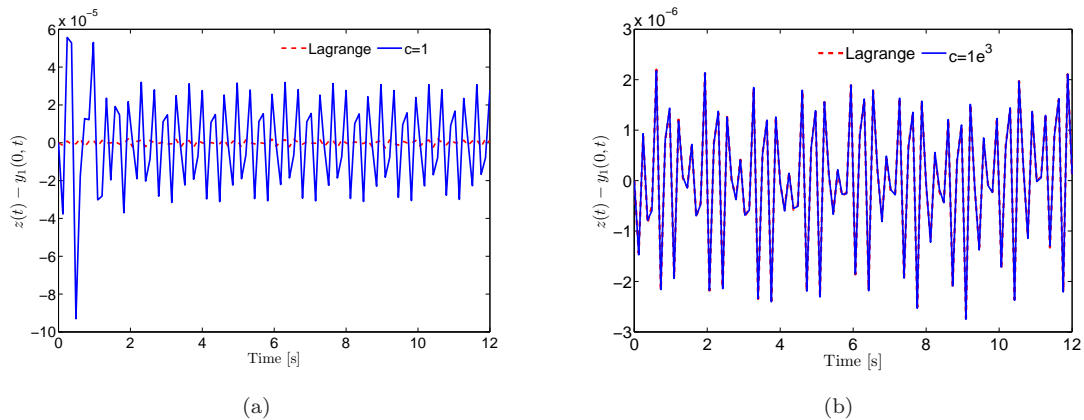


Figure 2.7: Comparison of the error between the Lagrange multiplier and the embedded boundary method for the second order dde (2.5.2) with (a) $c=1$ and (b) $c=1000$. The parameter values are the same as used to generate Figure 2.5.

2.7 Application to control

Numerical integration of a DDE using the dde23 solver will generally be faster than integrating a set of ODEs obtained using the Galerkin approximation. The real advantage of the proposed formulation lies in the design of observers, filters, and control systems for physical processes governed by DDEs. Modern control theory often assumes that the plant model can be approximated using ODEs, and several theoretical proofs are available for such models. Control theory for DDEs, on the other hand, is a topic of ongoing research [2], and the authors believe the field is underdeveloped. In this example, we apply the proposed boundary conditionfree formulation to a control problem to take advantage of control theory developed for systems described by ODEs.

Consider a process governed by following second order DDE:

$$\ddot{z} + 2\zeta\dot{z} + k_1z + k_2z(t - \tau) = 0 \quad (2.39)$$

where the parameters are $\zeta = 2$, $k_1 = 5$, $k_2 = 5$ and $\tau = 1$. The objective is to design an observer which can accurately track the response of the DDE (2.39). We obtain the plant output by integrating the DDE numerically using the following history functions:

$$z(t) = -1, \dot{z}(t) = 0, t \in [-1, 0] \quad (2.40)$$

We then use the approximated ODEs with history functions as $z(t) = 2, \dot{z}(t) = 0, t \in [-1, 0]$ to

track the plant response, whereupon traditional control strategies can be applied. Since Eq. (2.39) is a second order DDE, retaining N terms in the series approximation results in a system of (2.39) of $2N$ (corresponding to N displacements and N velocities). Inspired by the idea of high gain observer [37], we add $20(z(t) - y_1(0, t))$ to the first displacement level ODE and $20(\dot{z}(t) - y_2(0, t))$ to the first velocity-level ODE. Here, $y_1(0, t)$ and $y_2(0, t)$ indicate the observer output for displacement and velocity respectively. Finally, we integrate the ODEs forward in time and compare the plant and observer outputs. We then integrate the ODEs forward in time and compare the plant and observer outputs. As shown in Figure 2.8, the observer output $y_1(0, t)$ is in very good agreement with the plant output $z(t)$, and the tracking error quickly becomes negligible. This example clearly demonstrates that the proposed method can be used for control purposes (such as designing observers, filters, and controllers) for systems governed by retarded DDEs.

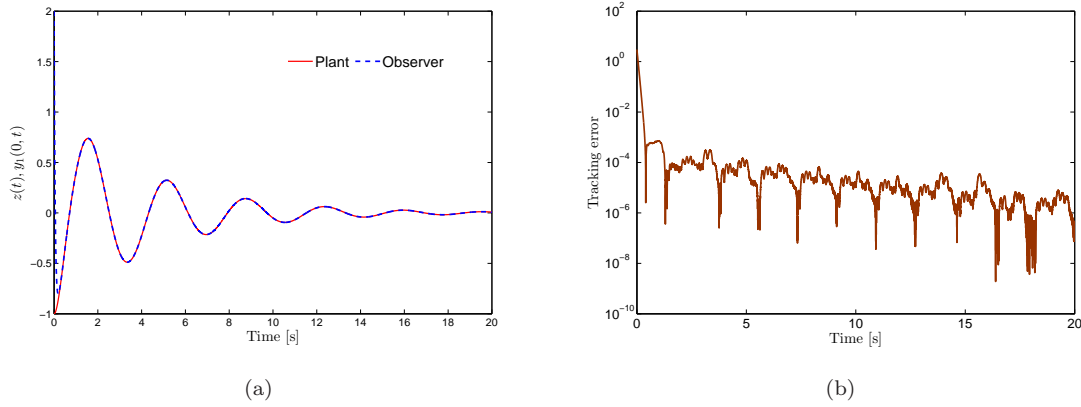


Figure 2.8: (a) Comparison of the plant output $z(t)$ and observer output ($y_1(0, t)$) for Eq. (2.39) (b) Tracking error as a function of time. The number of terms used in the galerkin series approximation are $N = 20$.

Chapter 3

Galerkin Methods for stability analysis with application to Bio-Mechanics

In this chapter we first present the mathematical model for the single-pendulum model of a human during stance (sagittal plane). Then we discuss our Galerkin method to determine the stability of the governing equation of motion. We derive analytical expressions of the stability boundary for this model and compare them with the numerical results. Next we develop the mathematical model for the PDA controlled double-pendulum model of a human during stance. We also derive analytical expressions for this model and compare them with the Galerkin results. Next we carry out extensive parametric studies to compare the PD- and PDA- controlled stability margins for this model. Finally we discuss the limitations of the analytical approach and the need of a numerical technique such as the proposed Galerkin method to determine the stability margins.

3.1 Mathematical Modeling

For clarity, we develop our theory on a single second-order neutral DDE; extension of the method to coupled DDEs is trivial. We first consider a single-pendulum model, as shown in Figure 3.1. The dynamics of this single-pendulum model are governed by the following second-order ODE [21]:

$$J_A \ddot{\theta}(t) + b_t \dot{\theta}(t) + k_t \theta(t) - mg\ell_{AC} \sin(\theta(t)) = Q(t) \quad (3.1)$$

where the pendulum is of mass m and length ℓ with orientation θ relative to vertical; J_A is the moment of inertia of the body about the ankle (point “A” in Figure 3.1); the passive torques applied by the plantarflexor and dorsiflexor muscles are lumped into a single torsional spring of stiffness k_t and a single torsional dashpot with damping coefficient b_t ; and g is the gravitational acceleration. $Q(t)$ is the feedback or active control torque required to prevent the human from falling, and can be expressed as follows:

$$Q(t) = -K_p \theta(t - \tau) - K_d \dot{\theta}(t - \tau) - K_a \ddot{\theta}(t - \tau) \quad (3.2)$$

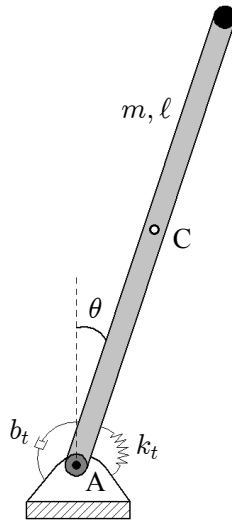


Figure 3.1: Single-pendulum model of a human during stance (sagittal plane). The body is represented by an inverted pendulum of mass m and length ℓ with orientation θ relative to vertical. Passive muscle torques generated at the ankle are modeled as a torsional spring of stiffness k_t and a torsional dashpot with damping coefficient b_t .

where τ is the reflex delay and K_p , K_d , and K_a are, respectively, the proportional (position), derivative (velocity), and acceleration control gains. The ODE in (3.1) becomes a DDE upon substitution of (3.2) due to the reflex delay τ . We linearize (3.1) about the vertical equilibrium point and define parameters $\alpha \triangleq b_t/J_A$, $\beta \triangleq (k_t - mg\ell_{AC})/J_A$, $k_p \triangleq -K_p/J_A$, $k_d \triangleq -K_d/J_A$, and $k_a \triangleq -K_a/J_A$ to obtain the following DDE:

$$\ddot{\theta}(t) + \alpha\dot{\theta}(t) + \beta\theta(t) = k_p\theta(t - \tau) + k_d\dot{\theta}(t - \tau) + k_a\ddot{\theta}(t - \tau) \quad (3.3)$$

The problem at hand is to determine the parameters for which (3.3) is stable. Substituting $\theta(t) = e^{rt}$, we obtain the following characteristic equation:

$$r^2 + \alpha r + \beta - (k_p + k_d r + k_a r^2) e^{-r\tau} = 0 \quad (3.4)$$

which is a quasi-polynomial and has infinitely many roots. The system is stable if, and only if, all the roots of the characteristic equation lie in the left half of the complex plane; however, verifying that all roots of (3.4) lie in the left half-plane is difficult, and this strategy will be impractical for more complex models. We instead determine the stability of an approximation to the DDE, a strategy that is equally suitable for low- and high-order models. We first introduce the following transformation:

$$y(s, t) = \theta(t + s) \quad (3.5)$$

where y is a function of s and t , and s varies from $-\tau$ to 0. Differentiating (3.5) with respect to s

and t , we obtain the following:

$$\frac{\partial y(s, t)}{\partial s} = \frac{\partial \theta(z)}{\partial z} \frac{\partial z}{\partial s} \Big|_{z=t+s} = \frac{\partial \theta(z)}{\partial z} \Big|_{z=t+s} \quad (3.6a)$$

$$\frac{\partial y(s, t)}{\partial t} = \frac{\partial \theta(z)}{\partial z} \frac{\partial z}{\partial t} \Big|_{z=t+s} = \frac{\partial \theta(z)}{\partial z} \Big|_{z=t+s} \quad (3.6b)$$

and note that $\partial y(s, t)/\partial s \equiv \partial y(s, t)/\partial t$. We now differentiate this relation with respect to time to obtain a second-order PDE:

$$\frac{\partial^2 y(s, t)}{\partial t^2} = \frac{\partial^2 y(s, t)}{\partial t \partial s}, \quad -\tau \leq s \leq 0 \quad (3.7)$$

Using relations $y(0, t) = \theta(t)$ and $y(-\tau, t) = \theta(t - \tau)$ obtained from (3.5), we derive the following boundary condition from (3.3):

$$\frac{\partial^2 y(0, t)}{\partial t^2} + \alpha \frac{\partial y(0, t)}{\partial t} + \beta y(0, t) = k_p y(-\tau, t) + k_d \frac{\partial y(-\tau, t)}{\partial t} + k_a \frac{\partial^2 y(-\tau, t)}{\partial t^2} \quad (3.8)$$

We now approximate the solution $y(s, t)$ of the PDE (3.7) as follows:

$$y(s, t) \approx \sum_{i=1}^N \phi_i(s) \eta_i(t) = \boldsymbol{\phi}^\top(s) \boldsymbol{\eta}(t) \quad (3.9)$$

where $\boldsymbol{\phi}(s) = [\phi_1(s), \phi_2(s), \dots, \phi_N(s)]^\top$ are the basis functions and $\boldsymbol{\eta}(t) = [\eta_1(t), \eta_2(t), \dots, \eta_N(t)]^\top$ are independent coordinates. In this study, we use the following shifted Legendre polynomials [38] as the basis functions:

$$\phi_1(s) = 1 \quad (3.10a)$$

$$\phi_2(s) = 1 + \frac{2s}{\tau} \quad (3.10b)$$

$$\phi_k(s) = \frac{(2k-3)\phi_2(s)\phi_{k-1}(s) - (k-2)\phi_{k-2}(s)}{k-1}, \quad k = 3, 4, \dots, N \quad (3.10c)$$

which are known to have better convergence properties than a mixed Fourier basis [35]. Substituting the approximate solution (3.9) into the PDE (3.7), we obtain the following:

$$\boldsymbol{\phi}^\top(s) \ddot{\boldsymbol{\eta}}(t) = \boldsymbol{\phi}^\top(s)' \dot{\boldsymbol{\eta}}(t) \quad (3.11)$$

where $\boldsymbol{\phi}^\top(s)' \equiv \partial \boldsymbol{\phi}^\top(s)/\partial s$. Pre-multiplying (3.11) by $\boldsymbol{\phi}(s)$ and integrating over s from $-\tau$ to 0, we arrive at a system of second-order ODEs:

$$\tilde{\mathbf{A}} \ddot{\boldsymbol{\eta}} = \tilde{\mathbf{B}} \dot{\boldsymbol{\eta}} \quad (3.12)$$

where $\tilde{\mathbf{A}} = \int_{-\tau}^0 \boldsymbol{\phi}(s) \boldsymbol{\phi}^\top(s) ds$ and $\tilde{\mathbf{B}} = \int_{-\tau}^0 \boldsymbol{\phi}(s) \boldsymbol{\phi}^\top(s)' ds$. Note that we can represent the solution using any complete set of basis functions (e.g., Chebyshev, Lagrange, and Hermite polynomials). In this work, we use shifted Legendre polynomials as global shape functions because they allow us to

write the entries of matrices $\tilde{\mathbf{A}}$ and $\tilde{\mathbf{B}}$ in closed form as follows:

$$\tilde{A}_{ij} = \frac{\tau}{2i-1} \delta_{ij} \quad i = 1, 2, \dots, N; j = 1, 2, \dots, N \quad (3.13a)$$

$$\tilde{B}_{ij} = \begin{cases} 2, & \text{if } i < j \text{ and } i + j \text{ is odd} \\ 0, & \text{otherwise} \end{cases} \quad i = 1, 2, \dots, N; j = 1, 2, \dots, N \quad (3.13b)$$

The boundary condition is enforced by first substituting the series solution (3.9) into (3.8):

$$\mathbf{a}\ddot{\boldsymbol{\eta}}(t) = \mathbf{b}\dot{\boldsymbol{\eta}}(t) + \mathbf{c}\boldsymbol{\eta}(t) \quad (3.14)$$

where $\mathbf{a} = \boldsymbol{\phi}^\top(0) - k_a \boldsymbol{\phi}^\top(-\tau)$, $\mathbf{b} = -\alpha \boldsymbol{\phi}^\top(0) + k_d \boldsymbol{\phi}^\top(-\tau)$, and $\mathbf{c} = -\beta \boldsymbol{\phi}^\top(0) + k_p \boldsymbol{\phi}^\top(-\tau)$. The boundary condition is incorporated into the system of ODEs using the tau method [35]. In this method, we replace the last row of (3.12) with (3.14):

$$\mathbf{A}\ddot{\boldsymbol{\eta}} = \mathbf{B}\dot{\boldsymbol{\eta}} + \mathbf{C}\boldsymbol{\eta} \quad (3.15)$$

where $\mathbf{A} = [\hat{\mathbf{A}}, \mathbf{a}]^\top$, $\mathbf{B} = [\hat{\mathbf{B}}, \mathbf{b}]^\top$, and $\mathbf{C} = [\mathbf{0}, \mathbf{c}]^\top$; matrices $\hat{\mathbf{A}}$ and $\hat{\mathbf{B}}$ are the matrices obtained by deleting the last row from matrices $\tilde{\mathbf{A}}$ and $\tilde{\mathbf{B}}$, respectively. Finally, we introduce the state vector $\mathbf{x} \triangleq [\boldsymbol{\eta}, \dot{\boldsymbol{\eta}}]^\top$ and write (3.15) in first-order form:

$$\dot{\mathbf{x}} = \mathbf{D}\mathbf{x} \quad (3.16)$$

where

$$\mathbf{D} = \begin{bmatrix} \mathbf{0} & \mathbf{1} \\ \mathbf{A}^{-1}\mathbf{C} & \mathbf{A}^{-1}\mathbf{B} \end{bmatrix} \quad (3.17)$$

In summary, we have converted the NDDE (3.3) into a system of first-order ODEs (3.16), the stability of which can be readily determined by examining the eigenvalues of matrix \mathbf{D} . If each eigenvalue of \mathbf{D} has a negative real part, then the system is stable. In fact, these eigenvalues approximate the characteristic roots of (3.4), and the approximation improves [35] as we increase the number of terms N in the series solution (3.9).

3.2 Results and Discussion

In this section, we first validate our developed method using a single-pendulum, sagittal-plane model of a human during quiet standing. We then extend our analysis to a double-pendulum model, which is governed by a system of coupled NDDEs. The analysis presented in Section 3.1 is applied to the first model directly, and can be readily extended to determine the stability of coupled NDDEs [20].

3.2.1 Single-pendulum human stance model

We first discuss the analytical results reported by Insperger et al. [21] for the single-pendulum human stance model. We then compare these results with those obtained using the Galerkin method

Parameter	Case 1	Case 2
m	60 kg	75.5 kg
ℓ_{AC}	1 m	0.92 m
J_A	60 kg m ²	63.9 kg m ²
k_t	471 Nm rad ⁻¹	595.5 Nm rad ⁻¹
b_t	4.0 Nms rad ⁻¹	4.011 Nms rad ⁻¹
τ	0.2 s	0.2 s

Table 3.1: Parameter values for single-pendulum human stance model. Insperger et al. [21] obtained these parameters from Asai et al. [39] (Case 1) and Loram and Lakie [40] (Case 2).

presented in Section 3.1.

Analytical stability margins

Recall the characteristic equation (3.4) for the single-pendulum model:

$$r^2 + \alpha r + \beta - (k_p + k_d r + k_a r^2) e^{-r\tau} = 0 \quad (3.18)$$

For constant-coefficient DDEs, the eigenvalues at the stability boundaries are purely imaginary; thus, we substitute $r = j\omega$ into (3.18):

$$-\omega^2 + j\alpha\omega + \beta - (k_p + jk_d\omega - k_a\omega^2) e^{-j\omega\tau} = 0 \quad (3.19)$$

Next, we expand $e^{j\omega}$ as $\cos(\omega) + j\sin(\omega)$ and separate the real and imaginary parts to obtain the following transcendental equations:

$$-\omega^2 + \beta - k_p \cos(\omega\tau) - k_d\omega \sin(\omega\tau) + k_a\omega^2 \cos(\omega\tau) = 0 \quad (3.20a)$$

$$\alpha\omega + k_p \sin(\omega\tau) - k_d\omega \cos(\omega\tau) - k_a\omega^2 \sin(\omega\tau) = 0 \quad (3.20b)$$

Using (3.20a) and (3.20b), we obtain the following closed-form expressions for k_p and k_d :

$$k_p = -\alpha\omega \sin(\omega\tau) + (-\omega^2 + \beta) \cos(\omega\tau) + k_a\omega^2 \quad (3.21a)$$

$$k_d = \frac{-\omega^2 + \beta}{\omega} \sin(\omega\tau) + \alpha \cos(\omega\tau) \quad (3.21b)$$

Thus, by varying parameter ω in (3.21), we can obtain the analytical stability boundaries for the PDA-controlled single-pendulum human stance model; to obtain the stability boundaries for the PD-controlled model, we simply set the acceleration gain $k_a = 0$ in (3.21a).

Galerkin stability margins

To validate the theory presented in Section 3.1, we have generated the stability diagrams for (3.1) using the parameters given in Table 3.1, and have compared our results with the analytical results discussed in Section 3.2.1 and reported by Insperger et al. [21]. The stability regions for Case 1 with PD and PDA controllers are shown in Figure 3.2 as the number of terms N in the series solution (3.9) increases. When $N = 5$, we obtain convergence with the analytical solution reported by Insperger et al. Table 3.2 confirms that the rightmost eigenvalue converges as we increase the number of terms

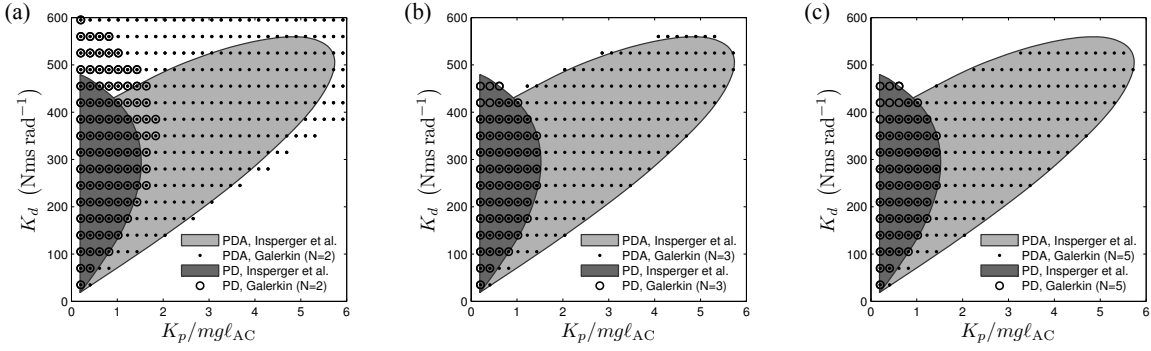


Figure 3.2: Stability regions for the single-pendulum human stance model (Case 1) using proportional-derivative (PD, open circles) and proportional-derivative-acceleration (PDA, filled circles) controllers, with (a) $N = 2$, (b) $N = 3$, and (c) $N = 5$ terms in the series solution. The shaded areas are the analytical stability regions reported by Insperger et al. [21]. The approximate Galerkin method converges to the analytical solution at $N = 5$. The parameters used in the simulation are $K_a = 54 \text{ Nms}^2 \text{ rad}^{-1}$ and those listed for Case 1 in Table 3.1.

Parameters		Rightmost eigenvalue		
K_p	K_d	$N = 3$	$N = 5$	$N = 7$
1764	600	$0.69 + 11.71i$	$0.70 + 11.21i$	$0.70 + 11.21i$
2940	600	$0.55 + 10.37i$	$0.65 + 10.01i$	$0.65 + 10.01i$
3528	600	$0.94 + 9.58i$	$1.03 + 9.35i$	$1.03 + 9.35i$

Table 3.2: Convergence analysis for the rightmost eigenvalue of the PDA-controlled single-pendulum human stance model. The values of parameters K_p and K_d are expressed in SI units; the values of all other parameters are as indicated in the caption for Figure 3.2.

N in the series solution (3.9).

We have also compared our results to those obtained by Insperger et al. for a second set of parameters (Case 2 in Table 3.1), shown in Figure 3.3. Once again, the proposed method converges to the analytical solution. These results confirm that the PDA controller provides a larger stability region than the PD controller for the sets of parameters we studied.

3.2.2 Double-pendulum human stance model

We now consider a double-pendulum human stance model in the sagittal plane, shown in Figure 3.4, where an additional active controller has been included at the hip. We assume that active torques are generated at the ankle and hip by continuous, time-delayed PDA feedback controllers to maintain an upright posture. We seek to determine whether the PDA controller remains superior to PD control for this two-degree-of-freedom human stance model, whose dynamics are more realistic than those of the single-pendulum model presented in Section 3.2.1.

After linearization, the dynamics of a double-pendulum model are governed by the following second-order ODE:

$$\mathbf{M}\ddot{\boldsymbol{\theta}} + \mathbf{C}\dot{\boldsymbol{\theta}} + \mathbf{K}\boldsymbol{\theta} = \mathbf{F} \quad (3.22)$$

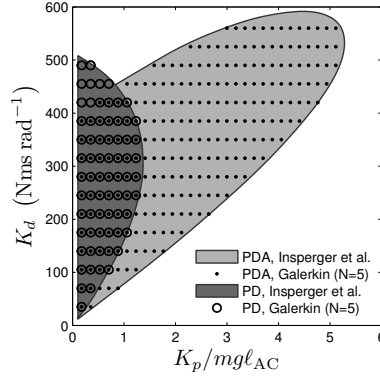


Figure 3.3: Stability regions for the single-pendulum human stance model (Case 2) using proportional–derivative (PD, open circles) and proportional–derivative–acceleration (PDA, filled circles) controllers. The shaded areas are the analytical stability regions reported by Insperger et al. [21]. The approximate Galerkin method converges to the analytical solution at $N = 5$. The parameters used in the simulation are $K_a = 57.51 \text{ Nms}^2 \text{ rad}^{-1}$ and those listed for Case 2 in Table 3.1.

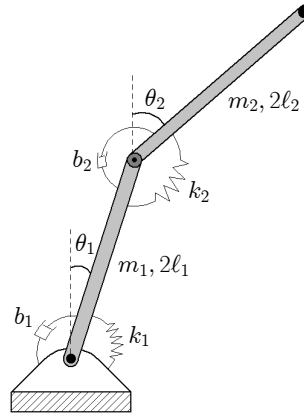


Figure 3.4: Double-pendulum model of a human during stance (sagittal plane). The lumped thigh and shank segment has mass m_1 , length $2\ell_1$, and orientation θ_1 relative to vertical; the knee is assumed to remain locked. The head, arms, and trunk are represented by a pendulum of mass m_2 and length $2\ell_2$ with orientation θ_2 relative to vertical. Passive muscle torques generated at the ankle and hip are modeled as torsional springs of stiffness k_1 and k_2 , respectively, and torsional dashpots with damping coefficients b_1 and b_2 .

where matrices \mathbf{M} , \mathbf{C} , and \mathbf{K} are defined as follows:

$$\mathbf{M} = \begin{bmatrix} J_1 + m_1\ell_1^2 + 4m_2\ell_1^2 & 2m_2\ell_1\ell_2 \\ 2m_2\ell_1\ell_2 & J_2 + m_2\ell_2^2 \end{bmatrix} \quad (3.23a)$$

$$\mathbf{C} = \begin{bmatrix} b_1 + b_2 & -b_2 \\ -b_2 & b_2 \end{bmatrix} \quad (3.23b)$$

$$\mathbf{K} = \begin{bmatrix} k_1 + k_2 - (m_1 + 2m_2)g\ell_1 & -k_2 \\ -k_2 & k_2 - m_2g\ell_2 \end{bmatrix} \quad (3.23c)$$

The lumped thigh and shank (leg) segment has mass m_1 , length $2\ell_1$, and moment of inertia J_1 about its centroid; the knee is assumed to remain locked. The head, arms, and trunk (HAT) are represented by a pendulum of mass m_2 , length $2\ell_2$, and moment of inertia J_2 about its centroid. Passive torques applied by the plantarflexor and dorsiflexor muscles at the ankle are lumped into a single torsional spring of stiffness k_1 and a single torsional dashpot with damping coefficient b_1 ; the hip flexors and extensors are modeled analogously. The time-delayed feedback torque \mathbf{F} in (3.22) is given by the following:

$$\mathbf{F} = -\mathbf{k}_p\boldsymbol{\theta}_{pos} - \mathbf{k}_d\dot{\boldsymbol{\theta}}_{vel} - \mathbf{k}_a\ddot{\boldsymbol{\theta}}_{acc} \quad (3.24)$$

where gain matrices \mathbf{k}_p , \mathbf{k}_d , and \mathbf{k}_a , and time-delayed state vectors $\boldsymbol{\theta}_{pos}$, $\dot{\boldsymbol{\theta}}_{vel}$, and $\ddot{\boldsymbol{\theta}}_{acc}$ are defined as follows:

$$\mathbf{k}_p = \begin{bmatrix} k_{p11} & k_{p12} \\ k_{p21} & k_{p22} \end{bmatrix}, \quad \mathbf{k}_d = \begin{bmatrix} k_{d11} & k_{d12} \\ k_{d21} & k_{d22} \end{bmatrix}, \quad \mathbf{k}_a = \begin{bmatrix} k_{a11} & k_{a12} \\ k_{a21} & k_{a22} \end{bmatrix} \quad (3.25a)$$

$$\boldsymbol{\theta}_{pos} = \begin{Bmatrix} \theta_1(t - \tau_p) \\ \theta_2(t - \tau_p) \end{Bmatrix}, \quad \dot{\boldsymbol{\theta}}_{vel} = \begin{Bmatrix} \dot{\theta}_1(t - \tau_v) \\ \dot{\theta}_2(t - \tau_v) \end{Bmatrix}, \quad \ddot{\boldsymbol{\theta}}_{acc} = \begin{Bmatrix} \ddot{\theta}_1(t - \tau_a) \\ \ddot{\theta}_2(t - \tau_a) \end{Bmatrix} \quad (3.25b)$$

In the following experiments, we use proportional gains $k_{p1} \triangleq k_{p11} = k_{p21}$ (ankle) and $k_{p2} \triangleq k_{p12} = k_{p22}$ (hip); similarly, the derivative gains are $k_{d1} \triangleq k_{d11} = k_{d21}$ and $k_{d2} \triangleq k_{d12} = k_{d22}$, and the acceleration gains are $k_{a1} \triangleq k_{a11} = k_{a21}$ and $k_{a2} \triangleq k_{a12} = k_{a22}$. The physical parameters used in Section 3.2.1 are distributed between the leg and HAT segments of the model to resemble the distribution in the human body [41]. In particular, 40% of the total mass is apportioned to the legs and 60% is assigned to the HAT segment. To maintain the same centroid position, the ratio of leg-to-HAT segment lengths is also 2:3.

Analytical stability margins

Substituting $\boldsymbol{\theta} = \boldsymbol{\theta}_0 e^{st}$ into (3.22), we obtain the following system of equations:

$$Z(s) = \mathbf{M}s^2 + \mathbf{C}s + \mathbf{K} + \mathbf{k}_p e^{-s\tau_p} + \mathbf{k}_d s e^{-s\tau_v} + \mathbf{k}_a s^2 e^{-s\tau_a} \quad (3.26)$$

For non-trivial solutions, the determinant of (3.26) must vanish—that is, we require $|Z(s)| = 0$. We use the Maple 16 computer algebra software to obtain the following characteristic equation

symbolically:

$$\begin{aligned}
& a_0s^4 + a_1s^3 + a_2s^2 + a_3s + a_4 + a_5s^4e^{-s\tau_a} + a_6s^3e^{-s\tau_a} + a_7s^3e^{-s\tau_v} + a_8s^2e^{-s\tau_a} \\
& + a_9s^2e^{-s\tau_v} + a_{10}s^2e^{-s\tau_p} + a_{11}se^{-s\tau_v} + a_{12}se^{-s\tau_p} + a_{13}e^{-s\tau_p} + a_{14}s^4e^{-2s\tau_a} \\
& + a_{15}s^2e^{-2s\tau_v} + a_{16}e^{-2s\tau_p} + a_{17}s^3e^{-s\tau_a}e^{-s\tau_v} + a_{18}s^2e^{-s\tau_a}e^{-s\tau_p} + a_{19}se^{-s\tau_v}e^{-s\tau_p} = 0 \quad (3.27)
\end{aligned}$$

The characteristic equation (3.27) is a quasi-polynomial; the coefficients $\{a_0, \dots, a_{19}\}$ have been reported in Appendix 4. Following a strategy similar to that discussed in Section 3.2.1, we now substitute $s = j\omega$ into (3.27):

$$\begin{aligned}
& a_0\omega^4 - ja_1\omega^3 - a_2\omega^2 + ja_3\omega + a_4 + a_5\omega^4e^{-j\tau_a\omega} - ja_6\omega^3e^{-j\tau_a\omega} - ja_7\omega^3e^{-j\tau_v\omega} \\
& - a_8\omega^2e^{-j\tau_a\omega} - a_9\omega^2e^{-j\tau_v\omega} - a_{10}\omega^2e^{-j\tau_p\omega} + ja_{11}\omega e^{-j\tau_v\omega} + ja_{12}\omega e^{-j\tau_p\omega} \\
& + a_{13}e^{-j\tau_p\omega} + a_{14}\omega^4e^{-j2\tau_a\omega} - a_{15}\omega^2e^{-j2\tau_v\omega} + a_{16}e^{-j2\tau_p\omega} - ja_{17}\omega^3e^{-j\tau_a\omega}e^{-j\tau_v\omega} \\
& - a_{18}\omega^2e^{-j\tau_a\omega}e^{-j\tau_p\omega} + ja_{19}\omega e^{-j\tau_v\omega}e^{-j\tau_p\omega} = 0 \quad (3.28)
\end{aligned}$$

Expanding the exponential terms and separating the real and imaginary parts yields the following two transcendental equations:

$$\begin{aligned}
& a_0\omega^4 - a_2\omega^2 + a_4 + a_5\omega^4 \cos(\tau_a\omega) - a_6\omega^3 \sin(\tau_a\omega) - a_7\omega^3 \sin(\tau_v\omega) - a_8\omega^2 \cos(\tau_a\omega) \\
& - a_9\omega^2 \cos(\tau_v\omega) - a_{10}\omega^2 \cos(\tau_p\omega) + a_{11}\omega \sin(\tau_v\omega) + a_{12}\omega \sin(\tau_p\omega) + a_{13} \cos(\tau_p\omega) \\
& + a_{14}\omega^4 \cos(2\tau_a\omega) - a_{15}\omega^2 \cos(2\tau_v\omega) + a_{16} \cos(2\tau_p\omega) - a_{17}\omega^3 \sin((\tau_a + \tau_v)\omega) \\
& - a_{18}\omega^2 \cos((\tau_a + \tau_p)\omega) + a_{19}\omega \sin((\tau_v + \tau_p)\omega) = 0 \quad (3.29a)
\end{aligned}$$

$$\begin{aligned}
& - a_1\omega^3 + a_3\omega - a_5\omega^4 \sin(\tau_a\omega) - a_6\omega^3 \cos(\tau_a\omega) - a_7\omega^3 \cos(\tau_v\omega) + a_8\omega^2 \sin(\tau_a\omega) \\
& + a_9\omega^2 \sin(\tau_v\omega) + a_{10}\omega^2 \sin(\tau_p\omega) + a_{11}\omega \cos(\tau_v\omega) + a_{12}\omega \cos(\tau_p\omega) - a_{13} \sin(\tau_p\omega) \\
& - a_{14}\omega^4 \sin(2\tau_a\omega) + a_{15}\omega^2 \sin(2\tau_v\omega) - a_{16} \sin(2\tau_p\omega) - a_{17}\omega^3 \cos((\tau_a + \tau_v)\omega) \\
& + a_{18}\omega^2 \sin((\tau_a + \tau_p)\omega) + a_{19}\omega \cos((\tau_v + \tau_p)\omega) = 0 \quad (3.29b)
\end{aligned}$$

where (3.29a) and (3.29b) are, respectively, the real and imaginary parts of (3.28). We next substitute all parameters except for the two gains in which we are interested, thereby obtaining expressions in terms of the two gains of interest and the parameter ω . Finally, we solve for the gains to obtain analytical expressions in terms of ω , then vary ω to obtain the stability boundaries. In the next section, we compute analytical stability boundaries using the above technique and compare them with the stability boundaries obtained using the Galerkin method presented in Section 3.1.

Galerkin stability margins

We now study several test cases using the parameters given in Table 3.3. Unless otherwise stated, we assume the position (τ_p), velocity (τ_v), and acceleration (τ_a) time delays are all equal to 0.05 s. Based on the convergence study shown in Table 3.4, we use $N = 5$ terms in the Galerkin series approximation (3.9). As shown in Figure 3.5, the stability boundaries obtained using the Galerkin and analytical approaches are in excellent agreement when $N = 5$ terms are used.

In Figures 3.6 and 3.7, we compare the stability diagrams for the PD- and PDA-controlled

Parameter	Value
m_1	28.36 kg
m_2	42.54 kg
ℓ_1	0.348 m
ℓ_2	0.522 m
ℓ	$(\ell_1 + \ell_2)$ m
J_1	1.145 kg m ²
J_2	3.864 kg m ²
k_1	217.7 Nm rad ⁻¹
k_2	250 Nm rad ⁻¹
b_1, b_2	4.011 Nms rad ⁻¹

Table 3.3: Parameter values for double-pendulum human stance model. Insperger et al. [21] obtained these parameters from Loram and Lakie [40]. The masses and lengths are distributed between the leg and HAT segments in a 2:3 ratio.

Parameters		Rightmost eigenvalue		
k_{p2}	k_{d2}	$N = 3$	$N = 5$	$N = 7$
12090	700	$7.66 + 37.86i$	$7.52 + 37.21i$	$7.52 + 37.21i$
12090	500	$3.32 + 32.33i$	$3.51 + 32.09i$	$3.51 + 32.09i$
9067.4	100	$4.09 + 19.57i$	$4.09 + 19.57i$	$4.09 + 19.57i$
3022.5	50	$1.68 + 12.38i$	$1.68 + 12.38i$	$1.68 + 12.38i$

Table 3.4: Convergence analysis for the rightmost eigenvalue of the PDA-controlled double-pendulum human stance model (3.22). The values of parameters k_{p2} and k_{d2} are expressed in SI units; the values of the other parameters are $k_{p1} = 1813$ Nm rad⁻¹, $k_{d1} = 300$ Nms rad⁻¹, $k_{a1} = k_{a2} = 10$ Nms² rad⁻¹, and those listed in Table 3.3.

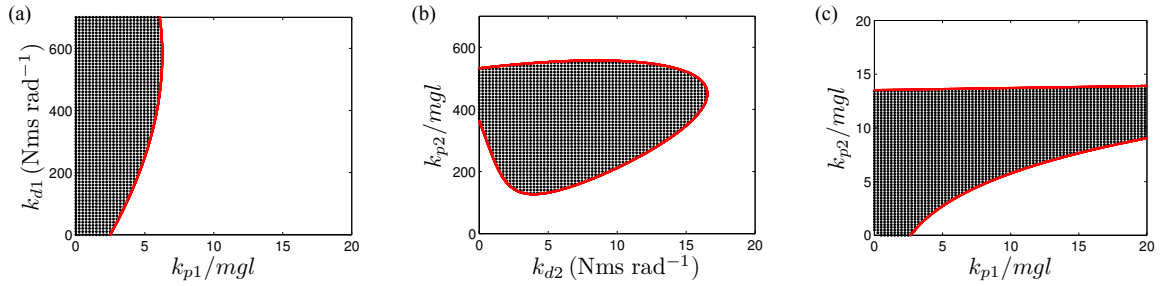


Figure 3.5: Stability regions obtained for the double-pendulum human stance model (3.22) using Galerkin and analytical approaches. The parameter values are (a) $k_{p2} = 1813$, $k_{d2} = 300$, $k_{a1} = k_{a2} = 10$; (b) $k_{p1} = 1813$, $k_{d1} = 300$, $k_{a1} = k_{a2} = 10$; and (c) $k_{d1} = k_{d2} = 300$, $k_{a1} = k_{a2} = 10$. Dots indicate stable points obtained using the Galerkin method and the solid red line indicates the analytical stability boundary.

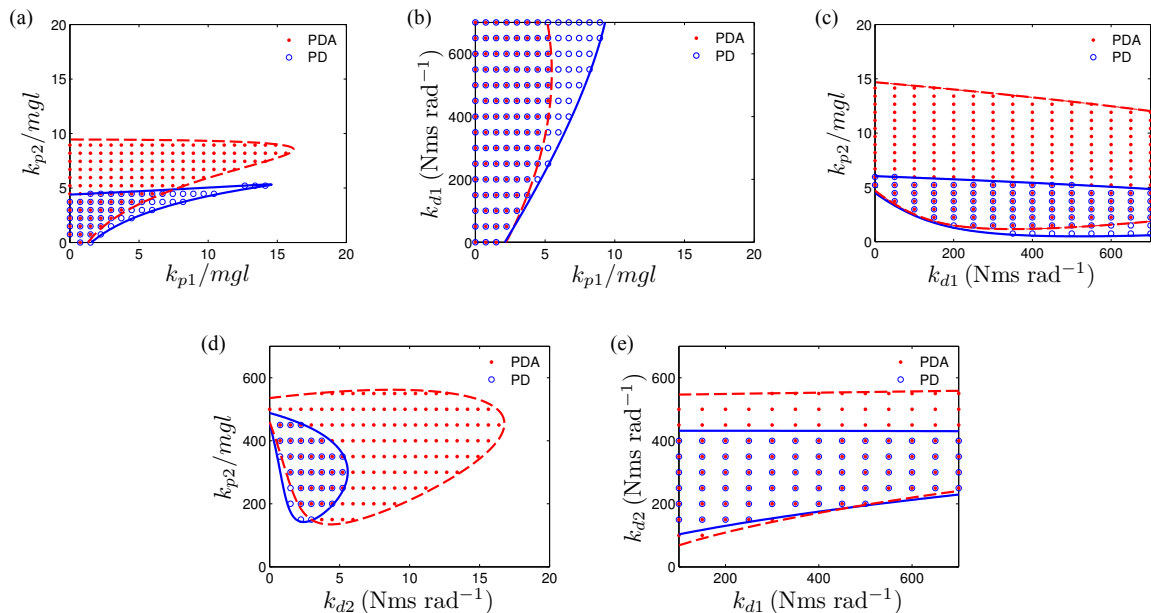


Figure 3.6: Stability regions obtained for the double-pendulum human stance model (3.22) using Galerkin and analytical approaches and the following parameters: (a) $k_{d1} = k_{d2} = 300$; (b) $k_{p2} = 1813$, $k_{d2} = 300$; (c) $k_{p1} = 1813$, $k_{d2} = 300$; (d) $k_{p1} = 1813$, $k_{d1} = 300$; and (e) $k_{p1} = 1813$, $k_{p2} = 2000$. The acceleration gains are $k_{a1} = 5$ and $k_{a2} = 10$ in all cases. Stable points obtained using the Galerkin method are indicated with red dots (PDA) and blue circles (PD); the analytical stability boundaries are indicated with dashed red (PDA) and solid blue (PD) lines.

double-pendulum human stance model with different gain combinations. We observe that the PDA controller provides larger stability regions than the PD controller, with the exception of the case shown in Figure 3.6(b). Finally, in Figure 3.8, we compare the PD and PDA stability regions for (3.22) with different combinations of the position (τ_p), velocity (τ_v), and acceleration (τ_a) time delays. Again, we find that the PDA-controlled model has larger stability regions than the PD-controlled model. These examples suggest that the PDA controller generally provides larger stability regions than the PD controller—that is, the double-pendulum human stance model will generally remain stable for a larger range of hip torque controller gains when acceleration feedback is included in the control scheme.

3.3 Limitations of the Analytical Approach

In this section, we discuss the limitations of the analytical approach and the need for a numerical technique such as the Galerkin method to determine the stability of the double-pendulum model. In Figure 3.9, we plot the analytical stability boundary obtained as the parameter ω in (3.28) is varied from 0 to 100. For both cases shown, we observe that the analytical solution has multiple branches as we sweep ω . These branches correspond to different roots crossing the imaginary axis. The problem at hand is illustrated in Figure 3.10: every root that is crossing the imaginary axis will satisfy (3.29), and it is impossible to determine which portion of this graph corresponds to the zone in which all roots lie in the left half of the complex plane. However, if we use the Galerkin method,

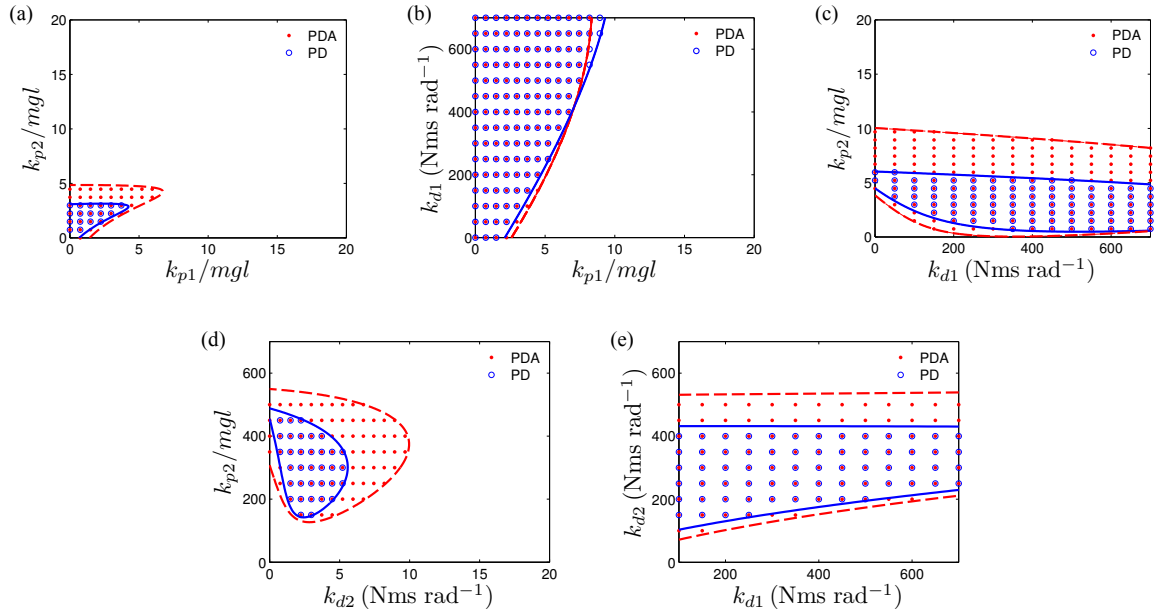


Figure 3.7: Stability regions obtained for the double-pendulum human stance model (3.22) using Galerkin and analytical approaches and the following parameters: (a) $k_{d1} = 300$, $k_{d2} = 150$; (b) $k_{p2} = 1813$, $k_{d2} = 300$; (c) $k_{p1} = 1813$, $k_{d2} = 300$; (d) $k_{p1} = 1813$, $k_{d1} = 300$; and (e) $k_{p1} = 1813$, $k_{p2} = 2000$. The acceleration gains are $k_{a1} = 10$ and $k_{a2} = 5$ in all cases. Stable points obtained using the Galerkin method are indicated with red dots (PDA) and blue circles (PD); the analytical stability boundaries are indicated with dashed red (PDA) and solid blue (PD) lines.

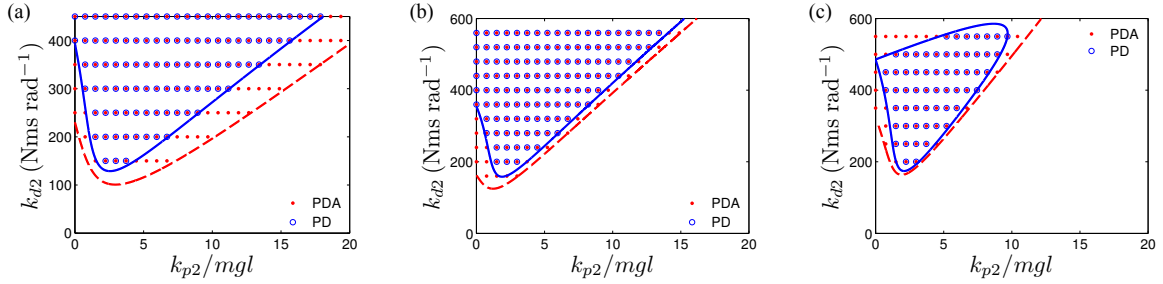


Figure 3.8: Stability regions obtained for the double-pendulum human stance model (3.22) using Galerkin and analytical approaches and the following position (τ_p), velocity (τ_v), and acceleration (τ_a) time delays: (a) $\tau_p = 0.05$, $\tau_v = 0.01$, $\tau_a = 0.09$; (b) $\tau_p = 0.09$, $\tau_v = 0.01$, $\tau_a = 0.05$; and (c) $\tau_p = 0.09$, $\tau_v = 0.05$, $\tau_a = 0.01$. The remaining parameters are the same as those used to generate Figure 3.7(d). Stable points obtained using the Galerkin method are indicated with red dots (PDA) and blue circles (PD); the analytical stability boundaries are indicated with dashed red (PDA) and solid blue (PD) lines.

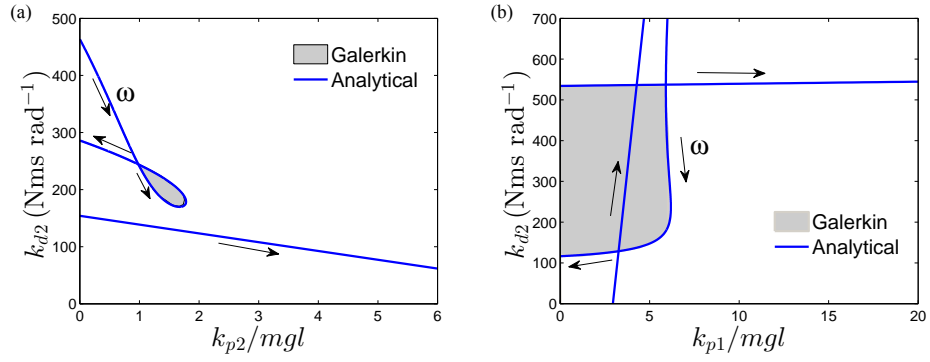


Figure 3.9: Stability margins obtained for the double-pendulum human stance model using Galerkin (shaded) and analytical (blue line) approaches with the following parameters: (a) $k_{p1} = 1813$, $k_{d1} = 300$, $k_{a1} = 10$, $k_{a2} = 5$, $\tau_p = 0.05$, $\tau_v = 0.09$, $\tau_a = 0.01$; and (b) $k_{p2} = 1813$, $k_{d1} = 300$, $k_{a1} = 10$, $k_{a2} = 5$, $\tau_p = \tau_v = \tau_a = 0.05$. Arrows indicate the direction of increasing ω .

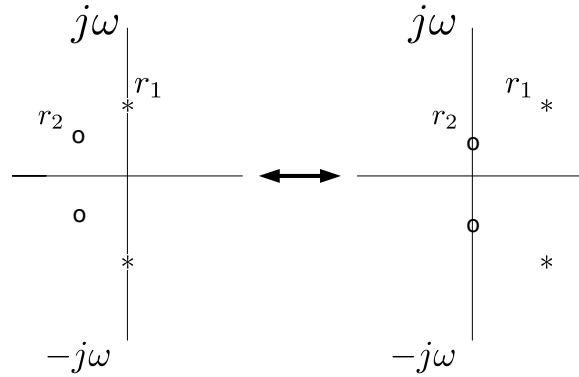


Figure 3.10: Possible locations of roots of the transcendental equation (3.29) for a given value of ω .

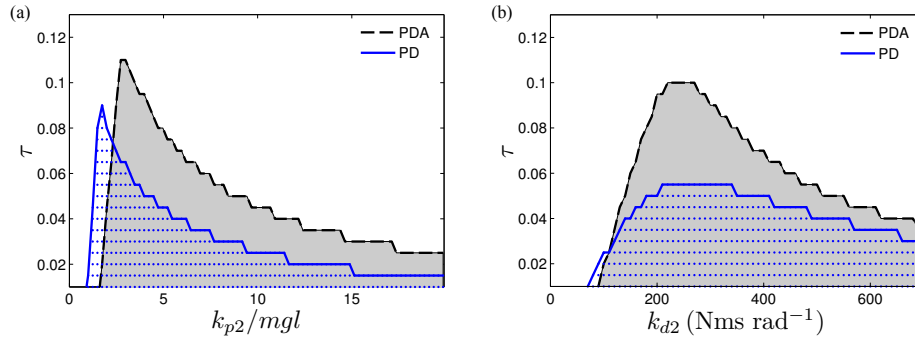


Figure 3.11: Stability regions obtained for the double-pendulum human stance model using the Galerkin method and the following parameter values: (a) $k_{p1} = 1813$, $k_{d1} = 300$, $k_{d2} = 200$, $k_{a1} = 5$, $k_{a2} = 10$; and (b) $k_{p1} = 1813$, $k_{p2} = 2000$, $k_{d1} = 300$, $k_{a1} = 5$, $k_{a2} = 10$. Stability regions are shown for PDA (shaded) and PD (dots) controllers.

we can precisely locate the stability regions without any ambiguity.

Finally, we investigate the stability regions as one gain and one time delay (τ) vary. Here, we assume equal position, velocity, and acceleration delays (i.e., $\tau \triangleq \tau_p = \tau_v = \tau_a$). Because τ appears as an argument to the trigonometric functions in (3.29), a stability diagram with τ as one of the varying parameters will involve multiple lobes corresponding to different periods of the trigonometric functions. In the cases shown previously (i.e., Figures 3.6 and 3.7) where two gains were varied, we observed that, for a given value of ω , we obtained linear expressions for the gains. In the present case, however, for a given value of ω , multiple solutions are possible because τ appears as an argument to trigonometric functions and the complexity of the model precludes obtaining an analytical expression in which τ is isolated. Thus, we must resort to a numerical strategy such as the proposed Galerkin method to determine the stability regions in this case. As shown in Figure 3.11, the stability regions obtained using the PDA controller are larger than those obtained using the PD controller—that is, the double-pendulum human stance model remains stable for larger time delays when acceleration feedback is included in the control scheme.

Chapter 4

Conclusions

We have, for the first time, transformed a given DDE into an equivalent PDE without any boundary conditions. This formulation allows us to apply the Galerkin method to the PDE without taking any special care to incorporate boundary conditions (using Lagrange multipliers or the tau method, for example). Legendre polynomials are used as the basis functions in the Galerkin method, and we ultimately obtain finite-dimensional ODE approximations of the original DDEs. We have demonstrated with several numerical examples that the ODEs obtained using our PDE formulation accurately capture the dynamics of the original DDEs. Convergence is attained by increasing the number of terms in the Galerkin approximation. We also observed that the proposed formulation approximates the Lagrange multiplier method for DDEs. An application of the proposed formulation was demonstrated to a problem of control. This formulation allows us to exploit existing tools developed for ODE systems to analyze DDEs.

As a second work, an approximate method to determine the stability of NDDEs has been developed to study the stability of human balance during stance. In particular, we use the Galerkin method to convert the governing NDDE into a system of ODEs and determine the stability of the latter, which is more tractable than determining the stability of the NDDE directly. We validated our method by reproducing the stability diagrams found analytically for a single-pendulum human stance model controlled by PD and PDA feedback controllers. We then derived analytical expressions for the stability boundaries of a PDA-controlled double-pendulum human stance model. The analytical and Galerkin stability boundaries were found to be in excellent agreement. Finally, we applied our method to determine the stability of the double-pendulum model.

The single-pendulum human stance model was found to have greater stability margins when acceleration feedback was available; for the double-pendulum model, we found that acceleration feedback generally—but not always—resulted in larger stability regions. These results corroborate those obtained by Insperger et al. [21] for the single-pendulum model, and further support the hypothesis that humans may, indeed, use a PDA control structure for maintaining balance, aided by sensory feedback from the vestibular system. As such, it may be crucial to include acceleration feedback in the controllers used by orthotic or prosthetic devices that assist persons with balance deficiencies [42]. It is also important to consider the complementary function of human muscle, which can begin reacting to disturbances even before reflexes respond [43]. Understanding the mechanisms of balance benefits the development of diagnostic criteria, assistive devices, and rehabilitation

strategies that will effectively support the growing elderly population.

References

- [1] R. D. Driver. Ordinary and Delay Differential Equations, volume 20 of *Applied Mathematical Sciences*. Springer, New York, 1977.
- [2] J.-P. Richard. Time-delay systems: an overview of some recent advances and open problems. *Automatica* 39, (2003) 1667–1694.
- [3] T. Insperger and G. Stépán. Stability of the milling process. *Periodica Polytechnica* 44, (2000) 47–57.
- [4] B. Balachandran. Nonlinear dynamics of milling processes. *Philosophical Transactions of the Royal Society A: Mathematical, Physical and Engineering Sciences* 359, (2001) 793–819.
- [5] M. P. Païdoussis. Fluid-Structure Interactions: Slender Structures and Axial Flow, volume 1. Academic Press, San Diego, 1998.
- [6] L. A. Safonov, E. Tomer, V. V. Strygin, Y. Ashkenazy, and S. Havlin. Multifractal chaotic attractors in a system of delay-differential equations modeling road traffic. *Chaos: An Interdisciplinary Journal of Nonlinear Science* 12, (2002) 1006–1014.
- [7] P. Wahi and A. Chatterjee. Galerkin projections for delay differential equations. *ASME Journal of Dynamic Systems, Measurement, and Control* 127, (2005) 80–87.
- [8] T. Koto. Method of lines approximations of delay differential equations. *Computers and Mathematics with Applications* 48, (2004) 45–59.
- [9] S. Maset. Numerical solution of retarded functional differential equations as abstract Cauchy problems. *Journal of Computational and Applied Mathematics* 161, (2003) 259–282.
- [10] A. H. Nayfeh and D. T. Mook. Nonlinear Oscillations. Wiley, New York, 1979.
- [11] W. F. J. Govaerts. Numerical Methods for Bifurcations of Dynamical Equilibria. Society for Industrial and Applied Mathematics, Philadelphia, 2000.
- [12] A. Dhooge, W. Govaerts, Y. A. Kuznetsov, H. G. E. Meijer, and B. Sautois. New features of the software MatCont for bifurcation analysis of dynamical systems. *Mathematical and Computer Modelling of Dynamical Systems* 14, (2008) 147–175.
- [13] C. P. Vyasarayani. Galerkin approximations for higher order delay differential equations. *ASME Journal of Computational and Nonlinear Dynamics* 7, (2012) 031,004.

- [14] K. Ito and R. Teglás. Legendre–tau approximations for functional-differential equations. *SIAM Journal on Control and Optimization* 24, (1986) 737–759.
- [15] A. de Jesus Kozakevicius and T. Kalmár-Nagy. Weak formulation for delay equations. In Proceedings of the 9th Brazilian Conference on Dynamics, Control and their Applications. Serra Negra, Brazil, 2010 732–736.
- [16] J. A. Stevens and E. D. Sogolow. Gender differences for non-fatal unintentional fall related injuries among older adults. *Injury Prevention* 11, (2005) 115–119.
- [17] A. J. Blake, K. Morgan, M. J. Bendall, H. Dallosso, S. B. J. Ebrahim, T. H. D. Arie, P. H. Fentem, and E. J. Bassey. Falls by elderly people at home: prevalence and associated factors. *Age and Ageing* 17, (1988) 365–372.
- [18] J. A. Stevens, P. S. Corso, E. A. Finkelstein, and T. R. Miller. The costs of fatal and non-fatal falls among older adults. *Injury Prevention* 12, (2006) 290–295.
- [19] B. Balachandran, T. Kalmár-Nagy, and D. E. Gilsinn. Delay Differential Equations: Recent Advances and New Directions. Springer, New York, 2009.
- [20] C. P. Vyasarayani. Galerkin approximations for neutral delay differential equations. *ASME Journal of Computational and Nonlinear Dynamics* 8, (2013) 021,014.
- [21] T. Insperger, J. Milton, and G. Stépán. Acceleration feedback improves balancing against reflex delay. *Journal of the Royal Society Interface* 10, (2013) 20120,763.
- [22] T. Kalmár-Nagy. Stability analysis of delay-differential equations by the method of steps and inverse Laplace transform. *Differential Equations and Dynamical Systems* 17, (2009) 185–200.
- [23] S. Yi and A. G. Ulsoy. Solution of a system of linear delay differential equations using the matrix Lambert function. In American Control Conference, 2006. IEEE, 2006 6–pp.
- [24] J. Milton, J. L. Cabrera, T. Ohira, S. Tajima, Y. Tonosaki, C. W. Eurich, and S. A. Campbell. The time-delayed inverted pendulum: implications for human balance control. *Chaos: An Interdisciplinary Journal of Nonlinear Science* 19, (2009) 026,110.
- [25] F. M. Atay. Balancing the inverted pendulum using position feedback. *Applied Mathematics Letters* 12, (1999) 51–56.
- [26] A. Bottaro, Y. Yasutake, T. Nomura, M. Casadio, and P. Morasso. Bounded stability of the quiet standing posture: an intermittent control model. *Human Movement Science* 27, (2008) 473–495.
- [27] K. H. Mauritz, V. Dietz, and M. Haller. Balancing as a clinical test in the differential diagnosis of sensory-motor disorders. *Journal of Neurology, Neurosurgery, and Psychiatry* 43, (1980) 407–412.
- [28] G. Stépán. Delay effects in the human sensory system during balancing. *Philosophical Transactions of the Royal Society A: Mathematical, Physical and Engineering Sciences* 367, (2009) 1195–1212.

- [29] R. Baratta and M. Solomonow. The dynamic response model of nine different skeletal muscles. *IEEE Transactions on Biomedical Engineering* 37, (1990) 243–251.
- [30] U. Proske and S. C. Gandevia. The proprioceptive senses: their roles in signaling body shape, body position and movement, and muscle force. *Physiological Reviews* 92, (2012) 1651–1697.
- [31] Y. Suzuki, T. Nomura, and P. Morasso. Stability of a double inverted pendulum model during human quiet stance with continuous delay feedback control. In Proceedings of the 33rd Annual International Conference of the IEEE Engineering in Medicine and Biology Society. Boston, Massachusetts, 2011 7450–7453.
- [32] R. Laube, S. Govender, and J. G. Colebatch. Vestibular-dependent spinal reflexes evoked by brief lateral accelerations of the heads of standing subjects. *Journal of Applied Physiology* 112, (2012) 1906–1914.
- [33] M. Roussel. Chemistry 5850: Nonlinear Dynamics, Lecture 11: Delay-differential equations. <http://people.uleth.ca/~roussel/nld/delay.pdf> .
- [34] L. F. Shampine and S. Thompson. Solving delay differential equations with dde23. <http://www.radford.edu/~thompson/webddes/tutorial.pdf> .
- [35] C. P. Vyasarayani, S. Subhash, and T. Kalmár-Nagy. Spectral approximations for characteristic roots of delay differential equations. *International Journal of Dynamics and Control* 2, (2014) 126–132.
- [36] T. Kalmár-Nagy, G. Stépán, and F. C. Moon. Subcritical Hopf bifurcation in the delay equation model for machine tool vibrations. *Nonlinear Dynamics* 26, (2001) 121–142.
- [37] H. K. Khalil. Nonlinear systems, 3rd. *New Jersey, Prentice Hall* 9.
- [38] I. S. Gradshteyn and I. M. Ryzhik. Table of Integrals, Series, and Products. 7th edition. Elsevier, Burlington, Massachusetts, 2007.
- [39] Y. Asai, Y. Tasaka, K. Nomura, T. Nomura, M. Casadio, and P. Morasso. A model of postural control in quiet standing: robust compensation of delay-induced instability using intermittent activation of feedback control. *PLoS ONE* 4, (2009) e6169.
- [40] I. D. Loram and M. Lakie. Direct measurement of human ankle stiffness during quiet standing: the intrinsic mechanical stiffness is insufficient for stability. *The Journal of Physiology* 545, (2002) 1041–1053.
- [41] B. Colobert, A. Crétual, P. Allard, and P. Delamarche. Force-plate based computation of ankle and hip strategies from double-inverted pendulum model. *Clinical Biomechanics* 21, (2006) 427–434.
- [42] J. Milton, J. L. Townsend, M. A. King, and T. Ohira. Balancing with positive feedback: the case for discontinuous control. *Philosophical Transactions of the Royal Society A: Mathematical, Physical and Engineering Sciences* 367, (2009) 1181–1193.

- [43] C. T. John, F. C. Anderson, J. S. Higginson, and S. L. Delp. Stabilisation of walking by intrinsic muscle properties revealed in a three-dimensional muscle-driven simulation. *Computer Methods in Biomechanics and Biomedical Engineering* 16, (2013) 451–462.

Appendix

The double-pendulum human stance model has the following characteristic equation (3.27):

$$\begin{aligned}
& a_0 s^4 + a_1 s^3 + a_2 s^2 + a_3 s + a_4 + a_5 s^4 e^{-s\tau_a} + a_6 s^3 e^{-s\tau_a} + a_7 s^3 e^{-s\tau_v} + a_8 s^2 e^{-s\tau_a} \\
& + a_9 s^2 e^{-s\tau_v} + a_{10} s^2 e^{-s\tau_p} + a_{11} s e^{-s\tau_v} + a_{12} s e^{-s\tau_p} + a_{13} e^{-s\tau_p} + a_{14} s^4 e^{-2s\tau_a} \\
& + a_{15} s^2 e^{-2s\tau_v} + a_{16} e^{-2s\tau_p} + a_{17} s^3 e^{-s\tau_a} e^{-s\tau_v} + a_{18} s^2 e^{-s\tau_a} e^{-s\tau_p} + a_{19} s e^{-s\tau_v} e^{-s\tau_p} = 0
\end{aligned}$$

where the coefficients are as follows:

$$\begin{aligned}
a_0 &= m_1 \ell_1^2 J_2 + 4m_2 \ell_1^2 J_2 + m_1 \ell_1^2 m_2 \ell_2^2 + J_1 J_2 + J_1 m_2 \ell_2^2 \\
a_1 &= 4m_2 \ell_1^2 b_2 + b_1 J_2 + 4m_2 \ell_1 \ell_2 b_2 + m_1 \ell_1^2 b_2 + b_2 m_2 \ell_2^2 + b_1 m_2 \ell_2^2 + J_1 b_2 + b_2 J_2 \\
a_2 &= -m_1 \ell_1^2 m_2 g \ell_2 - g \ell_1 m_1 m_2 \ell_2^2 + k_1 m_2 \ell_2^2 + m_1 \ell_1^2 k_2 + k_2 m_2 \ell_2^2 + 4m_2 \ell_1^2 k_2 - 2g \ell_1 m_2^2 \ell_2^2 \\
& + 4m_2 \ell_1 \ell_2 k_2 - J_1 m_2 g \ell_2 - 4m_2^2 \ell_1^2 g \ell_2 - g \ell_1 m_1 J_2 - 2g \ell_1 m_2 J_2 + k_1 J_2 + J_1 k_2 + b_1 b_2 + k_2 J_2 \\
a_3 &= -2g \ell_1 m_2 b_2 + k_1 b_2 + b_1 k_2 - b_1 m_2 g \ell_2 - b_2 m_2 g \ell_2 - g \ell_1 m_1 b_2 \\
a_4 &= -2g \ell_1 m_2 k_2 + 2g^2 \ell_1 m_2^2 \ell_2 - k_1 m_2 g \ell_2 - k_2 m_2 g \ell_2 - g \ell_1 m_1 k_2 + k_1 k_2 + g^2 \ell_1 m_1 m_2 \ell_2 \\
a_5 &= k_{a11} m_2 \ell_2^2 + J_1 k_{a22} - 2m_2 \ell_1 \ell_2 k_{a21} - 2k_{a12} m_2 \ell_1 \ell_2 + 4m_2 \ell_1^2 k_{a22} + m_1 \ell_1^2 k_{a22} + k_{a11} J_2 \\
a_6 &= k_{a12} b_2 + k_{a11} b_2 + b_2 k_{a22} + b_1 k_{a22} + b_2 k_{a21} \\
a_7 &= J_1 k_{d22} + k_{d11} m_2 \ell_2^2 + m_1 \ell_1^2 k_{d22} + 4m_2 \ell_1^2 k_{d22} - 2m_2 \ell_1 \ell_2 k_{d21} - 2k_{d12} m_2 \ell_1 \ell_2 + k_{d11} J_2 \\
a_8 &= -g \ell_1 m_1 k_{a22} - 2g \ell_1 m_2 k_{a22} - k_{a11} m_2 g \ell_2 + k_{a11} k_2 + k_1 k_{a22} + k_{a12} k_2 + k_2 k_{a21} + k_2 k_{a22} \\
a_9 &= k_{d11} b_2 + b_1 k_{d22} + b_2 k_{d22} + b_2 k_{d21} + b_2 k_{d12} \\
a_{10} &= m_1 \ell_1^2 k_{p22} + 4m_2 \ell_1^2 k_{p22} + k_{p11} m_2 \ell_2^2 - 2m_2 \ell_1 \ell_2 k_{p21} - 2m_2 \ell_1 \ell_2 k_{p12} + k_{p11} J_2 + k_{p22} J_1 \\
a_{11} &= k_1 k_{d22} - 2g \ell_1 m_2 k_{d22} + k_2 k_{d22} + k_2 k_{d11} - k_{d11} m_2 g \ell_2 - g \ell_1 m_1 k_{d22} + k_2 k_{d12} + k_2 k_{d21} \\
a_{12} &= b_1 k_{p22} + b_2 k_{p21} + b_2 k_{p11} + b_2 k_{p22} + b_2 k_{p12} \\
a_{13} &= -k_{p11} m_2 g \ell_2 + k_2 k_{p22} + k_{p12} k_2 - g \ell_1 m_1 k_{p22} + k_1 k_{p22} + k_{p11} k_2 + k_2 k_{p21} - 2g \ell_1 m_2 k_{p22} \\
a_{14} &= k_{a11} k_{a22} - k_{a12} k_{a21} \\
a_{15} &= k_{d11} k_{d22} - k_{d12} k_{d21} \\
a_{16} &= k_{p11} k_{p22} - k_{p12} k_{p21} \\
a_{17} &= -k_{d21} k_{a12} + k_{d11} k_{a22} + k_{a11} k_{d22} - k_{d12} k_{a21} \\
a_{18} &= k_{a11} k_{p22} - k_{p12} k_{a21} - k_{a12} k_{p21} + k_{p11} k_{a22} \\
a_{19} &= k_{d11} k_{p22} - k_{p12} k_{d21} + k_{p11} k_{d22} - k_{d12} k_{p21}
\end{aligned}$$